Studies on Layer-by-Layer Structures of Clay-Organic Hybrid Films

Kenji Tamura

1999

Studies on Layer-by-Layer Structures of

Clay-Organic Hybrid Films

Kenji Tamura

1999

Hokkaido University

ACKNOWLEDGMENTS

This thesis is a summary of the author's study during 1995-99 at the National Institute for Research in Inorganic Materials (NIRIM) in Tsukuba, and the Division of Biological Science, Graduate School of Science, Hokkaido University.

I would like to show my deep appreciation to my thesis supervisor, Professor Akihiko Yamagishi, Hokkaido University. Moreover I am greatly thankful to him for the assistance, encouragement, suggestion and helpful discussion for this work and this thesis. Further I am most grateful to Professor Yoichi Sasaki, Associate Professor Mitsuo Nakata, Hokkaido University, and Dr. Hiromoto Nakazawa, NIRIM, for their kind instructions and suggestions.

During the course of this work, I have profited greatly from Dr. Hiromoto Nakazawa, Dr. Hirohisa Yamada and Dr. Takayoshi Sasaki, NIRIM. I would like to express my cordial gratitude to them for their kind instruction, stimulated discussion, and continuous encouragement.

Thanks are due to the Showa Denko K.K. for giving me a chance to stay and study in Tsukuba: particularly, I thank Mr. Kiwami Hirota, Mr. Yoshihiro Motegi and Mr. Teruo Hosokawa .

I am indebted to the members of Professor Yamagishi's group for their help, useful discussions: especially, I thank Dr. Masahiro Taniguchi and Mr. Hitoshi Setsuda.

Finally, I thank heartily to my wife Keiko Tamura for her love and support.

February 1999

田村堅志

Kenji Tamura

CONTENTS

CHAPTER 1

GENERAL INTRODUCTION

1.1 Background

Ordered Molecular Thin Film

Molecular, ordered thin films, whose thickness ranges from a few nanometers (a monolayer) to several hundred nanometers, show considerable technological promise. Electronic and optical devices presently incorporate structures in this thickness range or approaching it, and organic thin films have been proposed to replace both passive and active components traditionally fabricated with other materials. Scientific studies of molecular interactions in thin-film structures have only recently been possible. The collective properties of ordered arrays have been characterized in more detail by a number of the newer surface science techniques.

The future for thin molecular solid lies in designing organized films to perform new and special functions. Of interest are arrays with the cooperative properties of the individual molecular components. Liquid crystal displays are a well-known example of a cooperative function, and much interest has focused on the nature of phase transitions and magnetism in two dimensions.

The area of Langmuir-Blodgett films, monolayer structures transferred from a water surface to a substrate, has recently been receiving a great deal of attention.[1-4] These films are appealing for study because of the facile manner in which a single monolayer or multilayers can be deposited. Such a capability brings to mind applications as organic superlattices created by the successive deposition of alternating layers of different molecules.[7-12] Another related topic is that of deposition from

solution through a chemical reaction at a surface to give a self-assembled system.[13-19]

All of this sounds exciting and promising, there are still many unsolved problems. For example, organic thin films suffer from fragility, impurities, and defects. Consequently, their use has been limited by the ability to produce films with good integrity, i.e., mechanical, thermal, and chemical stability, as well as with the desired properties. Efforts to overcome some of these problems have been progressing well. For strength, films are being polymerized, cross-linked and hybridization. Weak interactions, e.g., van der Waals forces, acid-base and charge-transfer interactions, and certain covalent chemical bonding, could be used to modify organic thin films more easily and to make molecular engineering and design changes.

Of particular interest is the preparation of highly ordered organic-inorganic ultrathin films in which an organic small molecule or a macromolecule is sandwiched between inorganic sheets. An inorganic layer is incorporated to reinforce the lamella structure of a film. One method of preparing such a hybrid film is bond chemically an inorganic sheet to an organic anchor which is self-assembled on a solid surface.[20] Multilayer formation is accomplished by bridging neighboring layers with a bifunctional agent. Another method is to deposit a polyelectrolyte and an inorganic layer alternatively onto solid substrate by immersing the substrate into their solutions.[21-26] A Layer-by-layer structure is maintained by electrostatic intercalation between oppositely charged layers.

In these attempt colloidal clay particle are expected to be useful for creating a new organic-clay nanostructure materials using self-assembly methods as chemical sensor, nonlinear optical device, electrode-modifiers and pyroelectric materials.[26-32] Their

properties depend on the properties of the organic molecules but also strongly on the physiochemical nature of clays. Despite of their importance, the nature of clay minerals has not fully understood due to inhomogeneous inter- and intra-charge distribution and impurity of materials. [33] The uncontrollable nature of natural clays results in the broad characters of organo-clay nanostructure films. Therefore it is important to understand the nature of clay minerals.

Clay Minerals

Clay minerals are distributed widely in nature and have been used in a variety of ways since the Stone Age. An important feature is the fact that the mineral crystal carries a negative charge, which is thought to be due to defects in the crystal lattice: some of the silicon (Si^{4+}) atoms are replaced by aluminum (Al^{3+}) and each such substitution produces one negative charge. An assembly formed by linking one tetrahedral sheet with one octahedral sheet is known as a 1:1 layer (Figure 1.1a). In such layers, the uppermost, unshared plane of anions in the octahedral sheet consists entirely of OH groups. Although isomorphous substitutions can take place in both component sheets, 1:1 layers must be electrostatically neutral overall. A 2:1 layer links two tetrahedral sheet with one octahedral sheet (Figure 1.1b). A 2:1 layer may be electrostatically neutral or may have an excess negative charge.

When dry montmorillonite is placed in a moist atmosphere, it is able to take up water between the triple-layer sheets. The first water molecules are associated with the interlayer cations and the hydration continues until two layers of water are contained

between each pair of sheets. The same degree of hydration occurs if a dry clay is placed in a concentrated (about 1 M) salt solution. If the salt concentration is lowered, the activity of the water is increased and more water can penetrate between the sheets and the clay mineral swells. The cation exchange and water adsorption behavior of clay minerals is very important in creating functional materials science.

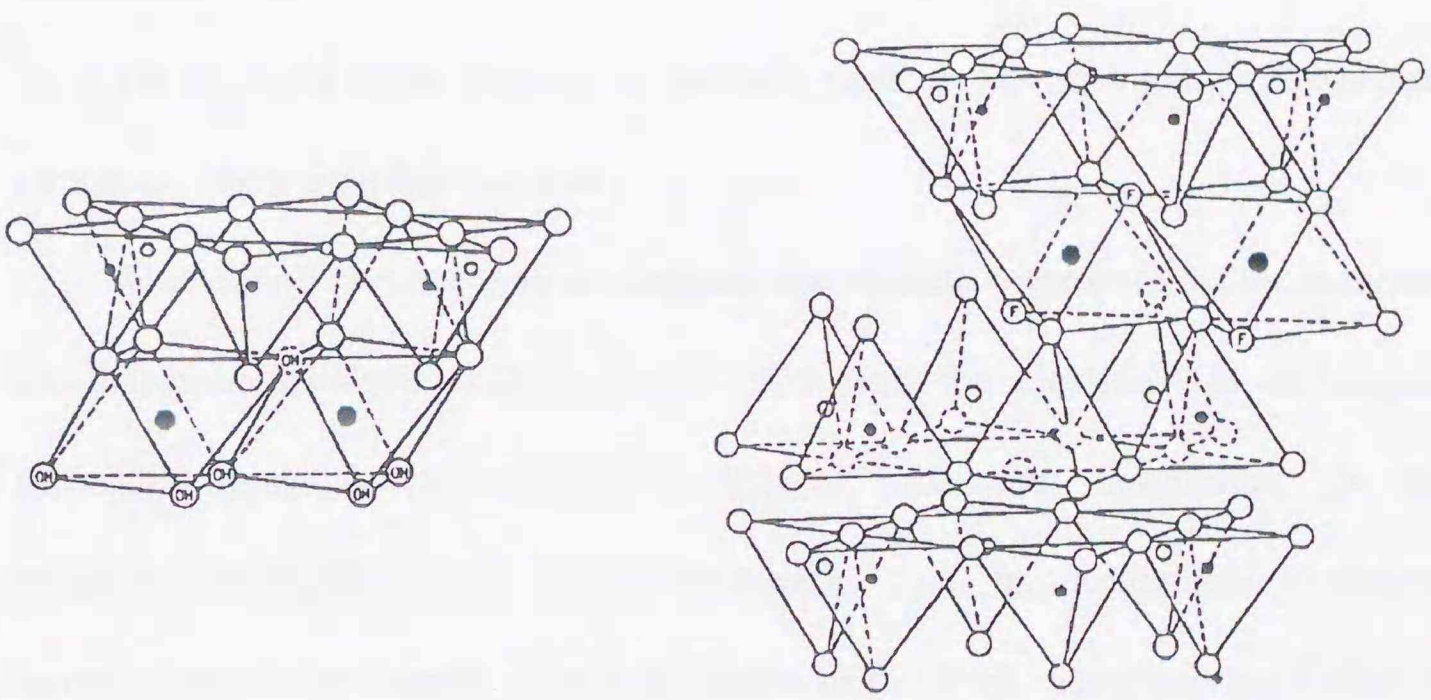

Figure 1.1 Typical structure of clay minerals

(a) 1:1 layer structure, (b) 2:1 layer structure

1.2 Purpose of this work

The first purpose was to investigate the nature of clay minerals such as a two stage expansion with increasing water and an intercalation properties of organic molecules. The materials used mainly in the present works are synthetic montmorillonite, synthetic taeniolite and synthetic hectorite having high crystallinity and homogeneous charge distribution. They are suitable as a model sample to study swelling process of clays by X-ray diffraction.

On the basis of the qualities of the bulk clays, a clay-organic hybrid structure was constructed in a water/air interface.

The second purpose was to elucidate the method to prepare a clay monolayer by the Langmuir-Blodgett (LB) method. Although the classical LB technique is a powerful approach to construct multilayer molecular assemblies, the method unfortunately suffers from critical drawbacks such as mechanical weakness and sensitivity to contaminates. As an extension of the work, our group has shown that an ultrathin hybrid film of a clay mineral and an amphiphilic metal complex can be built by using the LB technique. According to the method, a monolayer of an amphiphilic Ru(II) polypyridyl complex was formed onto an aqueous dispersion of a clay. The monolayer was used as template for adsorption of a clay particle. Ruthenium(II) polypyridyl complexes are known to be an efficient converter of photon energy.[34] Such a new hybrid film could be an important step towards the creation of organized layered compounds for controlling the deposition sequence and orientation of

intercalated molecules.

1.3 The Outline of the Thesis

In Chapter 2, the hydration behavior of clay were investigated by an *in situ* X-ray diffraction (XRD) technique using high crystallinty smectite with different exchangeable cations. In Chapter 3, osmotic swelling and reassembling behaviors of colloidal clay have been observed by an *in situ* XRD technique followed by a Laue function analysis. From this analysis, a structure of colloidal clay which was consist of a pair of the taeniolite sheets incorporating water, are determined. In Chapter 4, the intercalation experiments of clay minerals and quaternary ammonium cations were performed under controlled ion-exchange ratio. Detailed inspection of these XRD patterns clarified the structures of the complexes and also the intercalation mechanism. In Chapter 5, organized organic-inorganic ultrathin films were constructed from the fabrication of smectite unit layers and an amphiphilic ruthenium(II) complex monolayer films using conventional Langmuir-Blodgett (LB) technique. We investigated the effects of the particle size and charge density of smectite on the formation of LB hybrid thin film. In Chapter 6, the monolayer of a clay and a metal complex was transferred onto a hydrophilic glass plate to form a multilayer film of Z-type. The formation of an ordered film of ruthenium(II) complex/clay was confirmed by X-ray diffraction, UV-visible and FT-IR absorption spectra. Chapter 7 is the general conclusions of this study.

References

[1] Thin Solid Films **1980**, 68 (May 1).

[2] Thin Solid Films **1983**, 99 (Jan 14).

[3] Thin Solid Films **1980**, 132-134 (Oct-Dec).

[4] Roberts, G.G. *Adv.Phys.* **1985**, 34, 475.

[5] Barraud, A.; Rosilio, C.; Ruaudel-Teixier, A. *Thin Solid Films* **1980**, 68, 99; Solid State Technol. **1979**, August, 120.

[6] McCord, M.A.; Pease, R.F.W. *J.Vac.Sci.Technol,B* **1986**, 4, 86.

[7] Agarwal, D.K.; Srivastava, V.K. Solid State Commun. **1972**, 11, 1461.

[8] Roberts, G.G.; Petty, M.C.; Baker, S.; Fowler, M.T.; Thomas, N.J. *Thin Solid Films* **1985**, 132, 113.

[9] Sauteret, C.; Hermann, J.P.; Frey, R.; Pradere, F.; Ducuing, J.; Baughman, R.H.; Chance, R.R. *Phys.Rev.Lett.* **1976**, 36, 956.

[10] Kajzar, F.; Messier, J.; Zyss, J.; Ledoux, I. *Opt.Commun.* **1983**, 45, 13.

[11] Chollet, P.-A.; Kajzar, F.; Messier, J. *Thin Solid Films* **1985**, 132, 1.

[12] Decher, G. *Science* **1997,** *277,* 1232.

[13] Nuzzo, R.G.; Fusco, F.; Allara, D.L. *J.Am.Chem.Soc.* **1987**, 109, 2358.

[14] Gun, J.; Iscovici, R.; Sagiv, J. *J. Colloid Interface Sci.* **1984**, 101, 201.

[15] Maoz, R.; Sagiv, J. *J.Colloid Interface Sci.* **1984**, 100, 465.

[16] Allara, D.; Nuzzo, R.G. *Langmuir* **1985**, 1, 45.

[17] Maoz, R.; Sagiv, J. *Thin Solid Films* **1985**, 132, 135.

[18] See, for example: *Scientific American* **1977**, September.

[19] See, for example: *Proc.IEEE* 1985, 73(September).

[20] Rong, D.; Kim, Y.; Mallouk, T.E. *Inorg. Chem.* **1990,** *29,* 1531.

[21] (a) Kleinfeld, E.R.; Ferguson, G.S. *Science.,* **1994,** *265,* 370. (b) Kleinfeld, E.R.; Fergason, G.S. *Chem. Mater.* **1995,** *7,* 2327.

[22]Keller, S.W.; Kim, H-N.; Mallouk, T.E. *J. Am. Chem. Soc.,***1994,** *116,* 8817.

[23] Lvov,Y.; Ariga, K.;Ichinose, I.; Kunitake, T. *Langmuir* **1996,** *12,* 3038.

[24] Kimizuka, N.; Handa, T.; Ichinose, I.; Kunitake, T. *Angew. Chem. Int. Ed. Engl.* **1994,** *33,* 2483.

[25] Stain, A.; Kellar, S.W.; Mallouk, T.E. *Science* **1993,** *259,* 1558.

[26] Lvov, Y.; Ariga, K.; Ichinose, I.; Kunitake, T. *Langmuir* **1996,** *12,* 3038.

[27] Eaglesham, A.; Jaworek, T.; Cresswell, J.; Allen, S.; Brugess, A.; Ferguson, I.; Ryan, T.G.; Huchings, M.; Petty, M.C.; Yarwood, Y. *Langmuir* **1996,** *12,* 2292.

[28] Wijekoon, W.M.K.P.; Wijaya, S.K.; Bhawalkar, J.D.; Prasad, P.N.; Penner, T.L.; Armstrong, N.J.; Ezenyilimba, M.C.; Williams, D.J. *J. Am. Chem. Soc.,***1996,** *118,* 4480.

[29] Hicks, J.M.; Petralli-Mallow, T.; Byers, J.D. *Faraday Discuss.,* **1994,** *99,* 341.

[30] Olsson, U.; Nakamura, K.; Kunieda, H. *Langmuir* **1996,** *12,* 3054.

[31] Hotta, Y.; Taniguchi, M.; Inukai, K.; Yamagishi, A. *J. Electroannal. Chem.* **1997,** *429,* 107.

[32] Hotta, Y.; Inukai, K.; Taniguchi, M.; Yamagishi, A. *Clay Miner.* **1997**, *32,* 79.

[33] MacEwan, D. M. C.; Wilson, M. J. 1980. "*Crystal Structure of Clay Minerals and their X-ray Identification,*" Brindley, G. W.; Brown, G. eds. London: Mineralogical

Society, 197.

[34] Rotzinger, F.P.; Munavalli, S.; Comte, P.; Hurst, J.K.; Gratzel, M.; Pern, F.; Franck, A.J. *J. Am. Chem. Soc.,* **1987,** *109,* 6619.

CHAPTER 2

HYDRATION BEHAVIOR OF HIGH CRYSTARINITY SMECTITE WITH DIFFERENT EXCHANGEABLE CATIONS

ABSTRACT

Smectites synthesized at 5.5 GPa and 1500 °C had extremely high crystallinity and might have homogeneous charge distribution. The smectite was ion-exchanged with various cations (Na^+, Li^+, K^+, Ca^{2+} and Mg^{2+}) and the hydration behavior of each sample was observed by an *in situ* X-ray powder diffraction (XRD) method under precisely controlled relative humidity (RH). The smectite showed distinct stepwise (discontinuous) hydration against RH. During the transition between two hydration states, coexistence of the two states was observed. This suggests stoichiometric hydration of a smectite having homogeneous charge distribution and high crystallinity. Randomly interstratified structures of the 1- and 2-hydration states were also appeared as metastable phases, that was confirmed experimentally as a kinetic phenomena in hydration and dehydration processes.

2.1 Introduction

The interlayer hydration of smectites has been well studied under various relative humidities (RH). The role of the interlayer cation for that has been pointed out by many workers.[1]-[10] The variation in basal spacings of natural smectites is known to be caused by the variable number of water molecules equilibrated with relative humidity (RH) between the layers. The number of water layers ranges from zero to three. However, the hydration state of smectite is not always clearly defined, because X-ray observations for smectite at the same RH are scattered, as indicated by broad, irrational and asymmetrical *00l* reflections. These scattered observations have been interpreted as being caused by low crystallinity of smectite and inhomogeneous charge distribution in silicate sheets.[7]

Smectites synthesized at very high pressure and temperature (5.5 GPa and 1500 °C) have extremely high crystallinity [11] and may have homogeneous charge distribution.[12] Using such smectite is expected to be more advantageous than usual smectites for understanding interlamellar hydration of smectite. In this paper, the smectite was exchanged by various cations (Na^+, Li^+, K^+, Ca^{2+} and Mg^{2+}) and the hydration behavior of each sample was observed by an *in situ* X-ray powder diffraction (XRD) method under precisely controlled RH.

2.2 Experimental

Sample Preparation

The mineral phases coexisting with smectite in the very high pressure synthesis were identified by XRD method as described by Yamada et al.[13]. They were coesite, kyanite, a small amount of jadeite, and a small amount of mica. The smectite has high crystallinity : the full width at half maximum intensity (FWHM) of the (001) reflection is less than 1/3 that of natural smectite and is comparable to that of the other coexisting crystals.[11] This smectite is hereafter denoted as HCSm.

All the ion-exchange experiments were carried out at room temperature. Polyethylene tubes of 50 cm^3 were used to equilibrate the solid (30 mg) with the aqueous solution (25 cm^3) containing alkali metal and alkaline-earth metal chlorides. The tubes were agitated by a mechanical shaker at 200 strokes per min for 5 days. The materials were separated by centrifugation for 20 minutes at 15000 rpm.

XRD Observations under the Controlled RH

The swelling properties of HCSm were examined by an *in situ* XRD method under precisely controlled RH. The apparatus and the system used has been described elsewhere.[14] The principle of the apparatus is as follows: the sample holder of the powder X-ray diffractometer was covered by a stainless steel chamber having windows of polyimide film (Kapton® film) for incident and diffracted X-rays. The RH in the sample chamber was controlled by mixing of wet and dry nitrogen gas flows. About 60 minutes was necessary after changing RH for RH stabilization. The XRD samples

were prepared by orienting the ion-exchanged smectite and air-dried. In the case of Mg^{2+}-exchanged sample, XRD inspection was also made at 0% RH for those after various duration of drying (1 to 100 hours). XRD data were collected at a scan rate of 1.0 °2θ min^{-1} using Ni-filtered Cu*K*α radiation. The RH in the sample chamber was controlled from 0 to 95% and the temperature was fixed at 30 °C.

2.3 Results

XRD patterns are presented for the homoionic Na-, Li-, K-, Ca- and Mg-HCSms at intervals of 20% RH in the range 0 - 95% RH (Figures 2.1.a – 2.1.e), and *d*(001) peaks are plotted against RH (Figures 2.2.a – 2.2.e).

Na-HCSm.

The (001) spacings of Na-HCSm varied from 0.99 to 1.22, and finally to 1.50 nm as RH increased from 0 to 95% (Figure 2.1.a and 2.2.a). These values correspond to the 0-, 1-, and 2-layer hydration states respectively.

An (001) reflection doublet was observed during hydration state transition. An extremely weak reflection, marked by the broken line between the two peaks at 1.22 and 1.50 nm, appeared in the range of 20 - 95% RH. The peak shifted to 1.50 nm with increasing RH. The gradual change in the *d*-spacing indicates that hydration occurs through an increase in number of the 2-layer hydration state, which are randomly interstratified with the 1-layer hydration state.

All observed spacings are plotted against RH in Figure 2.2.a. A solid circle represents the basal spacing of the normal peak and an open circle that of the extremely weak reflection. The symbols **0W, 1W** and **2W** mean the 0-, 1-, and 2-layer hydration states and **R** means random. The shaded portion shows the range in which two phases coexist.

Li-HCSm.

Three hydration states, **0W, 1W,** and **2W,** appeared in the 0 to 95% RH range (Figure 2.1.b). Asymmetrical weak reflections also appeared between the 1.22 and 1.51 nm peaks in the range 0 to 95% RH. All observed spacings are plotted against RH in Figure 2.2.b. Coexistence of the **0W** and **1W** hydration states occurred in the range 20 to 30% RH and of the **1W** and **2W** states between 40 to 70% RH. The **R** phase was observed over a wide range, from 0 to 95% RH.

K-HCSm.

K-HCSm displayed broad, irrational and asymmetrical reflection over the entire RH range measured. Only two peaks, at 1.00 and 1.26 nm, were observed. The 1.00 nm spacing, corresponding to **0W,** predominated in the range 0 - 95% RH. Two hydration phases, the **0W** and **1W** states, were observed above 80% RH. The hydration curve plotted against RH shows distinct stepwise behavior (Figure 2.2.c).

Ca-HCSm.

XRD profiles for Ca-HCSm (Figure 2.1.d) showed sharper reflections compared

with those obtained from monovalent cations. The spacings of the three reflections were 1.20, 1.51 and 1.81 nm, corresponding to the 1-, 2-, and 3-layer hydration states. At 95% RH, a doublet composed of 1.51 (**2W**) and 1.81 nm (**3W**) basal spacings appeared. The plot of observed d-spacing vs. RH forms a slightly inclined line below 60% RH (Figure 2.2.d). The gradual change in the *d*-spacing indicates a randomly interstratified structure of **1W** and **2W** units. The phase is, thus, indicated by **R**.

Mg-HCSm.

The swelling behavior of Mg-HCSm was similar to that of the Ca-type. The hydration curve of Mg-HCSm indicated the presence of the R phase below 70% RH, and hydration states of **2W - 3W** above 80% RH. A single state of 3W appeared at 95% RH (Figure 2.2.e).

To check the relation between the R-phase and the hydration (**W**) phases, XRD patterns for Mg-HCSm prepared by allowing paste mounts to dry for times ranging from 1-16 hours, after dispersion of HCSm for ion-exchange were inspected (Figure 2.3). Mg-HCSm showed an asymmetrical (001) reflection profile (Figure 2.3, insertion). The asymmetry is due to the coexistence of two peaks at 1.36 nm (**R**-phase) and a shoulder peak at 1.25 nm (**1W**). The relative intensity of the two peaks defines the asymmetry which changes with increase in XRD sample preparation drying time. The ratio of I_R/I_{1W} was plotted against drying time (Figure 2.3).

2.4 Discussion

Stoichiometric Hydration of Smectite

Stepwise hydration is characteristic for all HCSm with various interlayer cations (Figure 2.1 and 2.2). Coexistence of two hydration states during transition exhibits stoichiometric hydration visually (Figure 2.2). Such stoichiometry in hydration is a behavior common in crystals having homogeneous charge distribution and high crystallinity, indicating that smectite is essentially crystalline and contains stoichiometric water molecules when its structure is as ideal as that of the present HCSm. The swelling of smectite has to be considered as a series of discontinuous phase transitions rather than as a continuous one as predicted by a recent molecular simulation.[15]

Randomly Interstratified Structure: An Intermediate Phase of the Stepwise Hydration

A weak and broad XRD reflection has been observed in the range 1.20 to 1.50 nm for Na^+ and Li^+ smectites (Figure 2.1.a and 2.1.b). The peak approaches 1.50 nm as RH increases. This can reasonably be explained by a randomly interstratified structure of **1W** (1.20 nm) and **2W** (1.50 nm) units. The structure formed when the original HCSm had been dispersed in alkaline solution for ion exchange and dried for XRD sample preparation. In the case of HCSm with divalent cations, the peak of the **R**-phase is dominant rather than those of the **1W** and **2W** phases (Figures 2.1.d, 2.1.e, 2.2.d and 2.2.e). The existence of the **R**-phase is supported by the following observations: (1) the d-value of the **R**-phase increases continuously with increasing RH (Figure 2.2),

(2) the peak has a shoulder at 1.20 nm corresponding to the *d*-value of the **1W**-phase (Figure 2.3, insertion), and (3) the intensity of the **R**-phase relative to that of the **1W**-phase decreases with increasing sample drying time after ion-exchange (Figure 2.3).

The drying experiment (Figure 2.3) indicates that the **R**-phase is an intermediate and metastable state too quick drying for segregation and growth of the thermodynamically stable phases. Given enough time, the crystal of Mg-HCSm might convert to the **1W** state entirely. Such a metastable state, once formed in sample preparation, keeps the random structure and increases its interlayer spacing continuously with increasing RH. The hydration force of the interlayer cation may dominantly affect the appearance of the **R**-phase. In fact, the amount of the **R**-phase relative to the stoichiometric phase increases in the order of K- < Na- < Li- < Ca- < Mg-HCSm. This order is consistent with the magnitude of hydration force of the interlayer cation.[16]

Comparison with Natural Smectite

There are some differences between the hydration behaviors of HCSm and those of natural smectites. Natural smectites do not show any stepwise hydration against RH, but rather continuous hydration.[8] This behavior is quite similar to that of the **R**-phase of HCSm. However, the origin of the randomness in layer stacking is probably different. In the natural smectites, it has been suggested to be due to inhomogeneous charge distribution in the silicate sheets and also due to small crystal size,[7] while in HCSm it is due to a kinetic phenomenon in the dehydration process as described above. The difference in the structure can also be seen in the fact that the basal spacing of Na-HCSm at 95% RH is 1.50 nm, corresponding to the **2W** state, but that of natural Na-

SWy is 2.33 nm, corresponding to a **3W** or more state.[8] This suggests that the interaction between the silicate layer and interlayer cations of HCSm with three dimensional periodicity might be stronger than that of "natural smectite" with inhomogeneous charge distribution.

2.5 Conclusion

The hydration behavior of HCSm with various exchangeable cations was observed by *in situ* XRD measurement under controlled RH. The basal spacing of HCSm varied stepwise with increasing RH, except for the **R**-phase, a random interstratified structure of **1W** and **2W**. Coexistence of two hydration states was observed in the XRD patterns as an (001) reflection doublet. These results clarified the stoichiometric hydration of the ideal smectite having a homogeneous charge distribution in the silicate layer. The appearance of the **R**-phases was a kinetic phenomenon in the hydration and dehydration processes which was largely controlled by the hydration force of cations in the interlayer.

Acknowledgment

The authors are indebted to Dr.H.Hashizume, NIRIM, for his cooperation for the *in situ* XRD measurement. Thanks are also due to Dr.J.R.Hester, NIRIM, for critical reading of manuscript and correction of English.

References

[1] Suquet, H.; Iiyama.J. T.; Kodama, H; Pezerat, H. *Clays Clay Miner* , **1977,** 25.

[2] Cebula, D.J.; Thomas, R. K.; Middleton, S.; Ottewill, R.H.; White, J.W.; *Clays Clay Miner* , **1979**, 27, 39.

[3] Hawkins, R.K.; Egelstaff, P. A.; *Clays Clay Miner* , **1980**, 28, 19.

[4] Sposito, G.; Prost, R. *Chem Rev* , **1982,** 82, 553.

[5] MacEvan, D. M. C.; Wilson, M. J. "*Crystal structures of clay and their X-ray identification,*" 1980: Brindley, G. W.; Brown, G. eds. London, Mineralogical Soc. p197.

[6] Moore, D. M.; Hower, J. *Clays Clay Miner* , **1986,** 34, 379.

[7] Watanabe, T.; Sato,T. *Clay Sci* , **1988,** 7, 129.

[8] Sato, T.; Watanabe, T.; Otsuka, R. *Clays Clay Miner,* **1992**, 40, 103.

[9] Güven, N. "*Clay-Water Interface and its Rheological Implications,*" 1992. Güven, N.; Pollastro, R. M. eds. Boulder, CO: Clay Miner Soc. p2-79.

[10] Bérend, I.; Cases, J. M.; François, M.; Uriot, J. P.; Michot, L.; Masion, A.; Thomas, F. *Clays Clay Miner* , **1995,** 43, 324.

[11] Nakazawa, H.; Yamada, H.; Fujita, T. *Appl Clays Sci* , **1992,** 6, 395.

[12] Yamada, H.; Nakazawa, H.; Hashizume, H.; Shimomura, S.; Watanabe, T. *Clays Clay Miner* , **1994,** 42, 77.

[13] Yamada, H.; Nakazawa, H.; Yoshioka, K.; Fujita, T. *Clay Miner* , **1991,** 26, 359.

[14] Hashizume, H.; Shimomura, S.; Yamada, H.; Fujita, T.; Nakazawa, H.; Akutsu, O. *Powder Diffraction* , **1996,** 11, 288.

[15] Karaborni, S.; Smit, B.; Heidug, W.; Urai, J.; van Oort, E. *Science,* **1996,** 271, 1102.

[16] Parker, J. C. *Soil physical chemistry,* Sparks, D.L. ed. Florida: CRS Press. p209-296.

CHAPTER 3

LAUE FUNCTION ANALYSIS OF COLLOIDAL LITHIUM TAENIOLITE

ABSTRACT

Osmotic swelling and reassembling behaviors of lithium taeniolite, $Li(Mg_2Li)Si_4O_{10}F_2$ (Li-TN), have been investigated by an *in situ* X-ray diffraction (XRD) technique under conditions where colloid concentration and drying speed were controlled. The *00l* reflections observed were characterized by a wavy distribution of intensity along 2θ without a flat region between the peaks. Profile analysis of the XRD pattern using Laue function indicated that the colloidal particle of Li-TN in dilute suspension consisted of a pair of the taeniolite sheets incorporating water. The peaks, *00l* reflections of the colloidal Li-TN, shifted to lower angle with increasing water concentration and to higher in drying process. The swelling and reassembling processes are discussed on the basis of the present model of the unit particle in suspension.

3.1 Introduction

Clay minerals exhibit a two stage expansion with increasing water. In the first, its layers expand discontinuously corresponding to number of water layers between clay sheets (crystalline swelling), whereas in the second stage, they expand continuously when contacted with water and yield finally a single layer colloidal suspension (osmotic swelling).[1] Osmotic swelling of clays such as montmollironite, vermiculite, and expandable mica has extensively been studied and has, over the years, been of great interest for soil scientists and those interested in fundamental properties of colloids.[1-17]

Recently it has been reported that colloidal clays are expected to be useful for creating a new organic-clay nanostructure materials as chemical sensor, nonlinear optical device, electrode-modifiers and pyroelectric materials.[18-22] Their properties, however, depend strongly on preparation of colloidal suspensions, which has not been fully understood. Some recent reports make partially clear a dynamic reassembling process for a layered protonic titanate using an *in situ* X-ray diffraction technique combined with Laue function analysis.[23, 24] If the technique is applied generally for the clay colloids, swelling mechanism of clays may be more deeply understood.

X-ray diffraction (XRD) method is the essential tool for studying swelling behavior of clay minerals. Several XRD methods and equipments have been developed for measuring the basal spacing of clay minerals in increasing water contents. Combination of XRD method and electro-chemical method has also been used for

understanding the relationship between the particle interlayer force and interlayer distance.[17] Despite those extensive works, the data are, however, not fully helpful in explaining swelling process because clay particles gave broad and scarce reflections in XRD pattern, except those synthesized under very high pressure and temperature.[25, 26]

A highly crystalline synthetic lithium taeniolite (Li-TN) was used in this work. Li-TN is an expandable mica and delaminates completely in water, being similar to smectites. The material is, therefore, suitable as a model sample to study swelling process of clays by X-ray diffraction. The purpose of this work is to investigate the swelling / restacking reactions and the colloidal structure in the processes of Li-TN by *in situ* X-ray diffraction method and Laue function analysis.

3.2 Experimental

Sample preparation.

Samples used were synthetic lithium taeniolite, $Li(Mg_2Li)Si_4O_{10}F_2$ (denoted by Li-TN; Topy Industries Co.,Ltd.). The cation exchange capacity (CEC) was 157 ± 9 meq/100g by the ammonium acetate adsorption method.[27] A fraction of 0.9 μm median particle size was separated by sedimentation and used throughout the study. Colloidal samples were prepared by mixing Li-TN powder and distilled water in variable solid/water ratio. They were stable for several weeks. Water contents of their suspensions were reexamined before the *in situ* XRD measurements.

In situ XRD techniques.

The XRD data were collected using a X-ray powder diffractometer equipped with a horizontal sample stage and a humidity/temperature controllable chamber (Rigaku RINT 2000S, Graphite monochromatic Cu-Kα radiation, slits: 0.5°, 0.5° and 0.15 mm).[28] The diffraction geometry was calibrated using 1-tetradecanol for lower angle of 2θ and Si powder for higher.[29]

The XRD data of Li-TN in various suspensions were obtained under following conditions: (i) the aqueous samples for different concentrations were subjected to XRD measurements, which were covered with polyester film of 4 μm thickness to avoid water evaporation during experiments, and (ii) colloidal aggregate centrifuged from a suspension was subjected to the in situ XRD measurement under a fixed relative humidity of 90 % and temperature of 30°C for observing the change in sluggish drying.

3.3 Results

In situ XRD measurements.

Typical XRD patterns of Li-TN suspensions in increasing and decreasing water content were shown in Figure 3.1 and 3.2, respectively. All diffraction peaks were well defined but were characterized by wavy distribution of intensity along 2θ. Especially, those of highly hydrated states showed oscillating profiles without flat bottom between the peaks suggesting extremely thin nature of colloid particles (Figure 3.1c, 3.1d, and 3.2

a-c). With increasing water, *00l* reflections shifted to lower angle and the background around the peaks increases simultaneously. The d-spacings of *00l*, *l* =2, 3 and 4, observed for the suspension of $[H_2O]/[Li\text{-}TN]=6.4$ were 5.6, 3.8, and 2.9 nm, respectively, which indicated that the intersheet separation is as high as 12 nm. When the $[H_2O]/[Li\text{-}TN]$ ratio was higher than 8.0, the diffraction peaks were not observed (Figure 3.1(e)).

By slow drying of the sample at relative humidity of 90%, the basal reflections were shifted to higher angle and finally a crystalline phase having an interlayer spacing of 1.9 nm were appeared which indicated 3 water layers in the intersheet (Figure 3.2 (d)).

The basal spacings observed are plotted against the weight ratio of $[H_2O]/[Li\text{-}TN]$ in Figure 3.3. Solid symbols are those obtained from XRD data represented in Figure 3.1 and open symbols are those not represented. The basal spacing increased linearly from 3.4 nm to 13.0 nm with increasing water. Reverse relation was seen for drying process at a fixed relative humidity of 90% (Figure 3.4). The open triangles in Figure 3.4 indicate the d-spacings of less hydrated phases appeared as the additional peaks due to heterogeneous drying of the sample, probably at the surface.

X-ray profile analysis.

XRD patterns of Li-TN in highly hydrated states (4.0 to 7.0 in $[H_2O]/[Li\text{-}TN]$ ratio) showed oscillating profile without flat bottom between peaks (Figure 3.1(c), 3.1(d) and 3.2(a)-3.2(c)). The oscillating profile implies that only very limited number of taeniolite layers were stacked. Similar pattern has been reported by Sasaki et al. for the protonic titanate in a highly hydrated state.[23] The diffraction feature has been

discussed in terms of profile simulation with Laue function. This procedure is applied to the present system.

In order to obtain accurate information, the *00l* diffraction patterns were numerically simulated for the system of N parallel taeniolite sheets with the spacing of d_{001} using following equations.

$$I(\theta) = \frac{1+\cos^2 2\theta}{\sin^2\theta \cdot \cos\theta} \cdot F^2(\theta) \cdot \frac{\sin^2\left(2\pi N d_{001}\sin\theta/\lambda\right)}{\sin^2\left(2\pi d_{001}\sin\theta/\lambda\right)} \qquad [1]$$

where the first, second and third terms are the Lorentz-polarization factor, structure factor and interference function, respectively. The notations, θ and λ, are the scattering angle and the X-ray wavelength, respectively. N is the number of periodic lattice which is concerned to their reflections.

The structure factor was calculated on the basis of the model (Figure 3.3) which comprises two parallel 2:1 layers of Li-TN with liquid water between them. The structure model of the layer is referred to that of K-TN single crystal analysis by Toraya et al.(1977) [30]. The scattering power of the intersheet water was modeled as uniform electron density for liquid water[23] and calculated by the integration below. Hence the structure factor *F(θ)* of the highly swollen Li-TN was described as follows;[23, 30]

$$
\begin{aligned}
F(\theta) = 2\int_0^{dw/2} \left(\frac{f_0}{0.623}\right)\cdot\cos 2\pi(2z\sin\theta/\lambda)dz \\
+4f_{Mg}\cos 2\pi(d_{001}\cdot\sin\theta/\lambda) \\
+2f_{Li}\cos 2\pi(d_{001}\cdot\sin\theta/\lambda) \\
+8f_O\cos 2\pi\left[2(d_{001}-0.11)\sin\theta/\lambda\right] \\
+4f_F\cos 2\pi\left[2(d_{001}-0.11)\sin\theta/\lambda\right] \\
+8f_{Si}\cos 2\pi\left[2(d_{001}-0.27)\sin\theta/\lambda\right] \\
+12f_O\cos 2\pi\left[2(d_{001}-0.33)\sin\theta/\lambda\right] \qquad [2]
\end{aligned}
$$

where f_{Mg}, f_{Li}, f_O, f_F, and f_{Si} are the atomic scattering factors corresponding to Mg, Li, O, F, and Si in Li-TN, respectively. The first term is the contribution from water of thickness d_W in gallery of taeniolite layer. Since the structure has a center of symmetry with respect to z=0, only cosine terms are taken into account. The contribution from exchangeable Li ion is negligibly small because of its small scattering power, and its low population in comparison with the number of water molecules.

Simulated XRD patterns are shown for d_{001} = 8.0 nm, and N=1, 2, 3 in Figure 3.6a. The similar line profile extracted from the observed patterns is also superposed on the simulation (Figure 3.6(b)). As shown in Figure 3.6b, the XRD pattern observed shows a close match to the calculated pattern for N=1 in terms of oscillating line profile as well as FWHM for *00l* reflections. Therefore, the XRD patterns indicate that the unit particle of Li-TN suspension is a pair of the taeniolite sheets incorporating water (Figure 3.5).

3.4 Discussion

The present XRD experiments and analysis has made clear the structure of the unit particle which appears during the osmotic swelling of Li-TN. The particle is consisted with two parallel sheets of 2:1 taeniolite layer and the intersheet water of variable thickness depending on the water/solid ratio. The suspension is the system of the particles oriented randomly each other and external water as solution. Such particle appears in rather dilute suspension of the water/solid ratio between 4.0 and 8.0 (Figure 3.1(c) and 3.1(d)). When the ratio exceeds over 8.0, the sheets do not keep their parallel arrangement and are cleaved into individual sheet. This can be seen in its XRD profile without any peaks (Figure 1(e)) as suggested previously in the text by van Olphen (1977).[1]

Swelling structure in the suspension of lower water/solid ratio (<4.0) is an intermediate and may be more complicated structure between the present two-sheet model and crystalline structure of turbostratic stacking. There may be two explanations for the structure; (1) the crystalline stacking is inserted randomly by the two-sheet structure in increasing water/solid ratio, and (2) the water is homogeneously but somewhat irregularly inserted in every interlayer. These two models explain similarly their XRD profiles (Figure 3.1(a) and 3.1(b)) that exhibit broader peaks and larger FWHM of peaks in higher indices due to disorder in the interlayer spacing.

Swelling of montmorillonite has extensively been studied for explaining the relation between the d-spacing and the solid/water ratio.[3,4,9] However, XRD patterns commonly known shows no sharp and higher order *00l* reflections. Since the

particle size of natural montmorillonite is far smaller than that of the present Li-TN, the broadening and disappearance of higher *00l* reflections may be regarded as much more distortion of the interlayer spacing due to the difficulty in keeping silicate sheet parallel. This suggests that the present model may also be applicable to explain the relationship between the d-spacing and solid/water ratio of natural montmorillonite taking into account the XRD profile.

Between crystalline and osmotic swelling, a jump of basal spacing from 1.9 to 4.0 nm is well known for Na-montmorillonite, whereas Li-montmorillonite does not show such discontinuous change similar to that of the present Li-TN (Figure 3.3 and 3.4).[1-3], [14] If the present model is completely applicable to the natural smectite, the different behaviors may be attributed to the potential difference from a crystalline stacking of 2:1 layers to the unit particles of colloid, which may be largely affected by the internal cations.

References

[1] van Olphen, H. *An Introduction to Clay Colloid Chemistry,* 2nd ed; Wiley: New York, 1977.

[2] Norrish, K. *Faraday Soc. Discuss.* **1954,** *18,* 120.

[3] Foster, W.R.; Savins, J.G.; Wait, J.M. *Clays Clay Miner* **1955,** *3,* 296.

[4] MacEvan, D.M.C.; Wilson, M. *Crystal Structures of Clay and their X-ray Identification*; Mineralogical Society: London, 1980.

[5] Cebura, D, J.; Thomas, R. K.; Middleton, S.; Ottewill, R. H.; White, J. W. *Clays Clay Miner.* **1979,** *27,* 39.

[6] Sposito, G.; Prost, R. *Chem. Rev.* **1982,** *82,* 553.

[7] Mulla, D.J.; Low, P.F. *J. Colloid Interface Sci.* **1983,** *95,* 51.

[8] Viani, B.E.; Low., P.F.; Roth, C.B.*J. Colloid Interface Sci.* **1983,** *96,* 229.

[9] Fukushima, Y. *Clays Clay Miner* **1984,** *32,* 320.

[10] Viani, B.E.; Roth, C.B.; Low., P.F. *Clays Clay Miner* **1985,** *3,* 244.

[11] Wu, J.; Low, P.F.; Roth, C.B. *Clays Clay Miner.* **1989,** *37,* 211.

[12] Vali, H.; Hesse, R.; Kohler, E.E., *Clays Clay Miner.* **1992,** *40,* 620.

[13] Gu, B.; Doner, H.E. *Clays Clay Miner.* **1992,** *40,* 246.

[14] Güven, N. *Clay-Water Interface and its Rheological Implications*; The Clay Minerals Society: 1992.

[15] Gu, B.; Doner, H.E. *Clays Clay Miner.* **1993,** *41,* 114.

[16] Zhang, F; Low, P. F.; Roth, C. B. *J. Colloid Interface Sci.* **1995,** *173,* 34 .

[17] Tateyama, H.; Scales, P.J.; Ooi, M.; Nishimura, S.; Rees, K.; Healy, T.W. *Langmuir* **1997,** *13,* 2440.

[18] Lvov, Y.; Ariga, K.; Ichinose, I.; Kunitake, T. *Langmuir* **1996,** *12,* 3038.

[19] Olsson, U.; Nakamura, K.; Kunieda, H. *Langmuir* **1996,** *12,* 3054.

[20] Kleinfeld, E.R.; Fergason, G.S. *Chem. Mater.* **1995,** *7,* 2327.

[21] Hotta, Y.; Taniguchi, M.; Inukai, K.; Yamagishi, A. *J. Electroannal. Chem.* **1997,** *429,* 107.

[22] Hotta, Y.; Inukai, K.; Taniguchi, M.; Yamagishi, A. *Clay Miner.* **1997,** *32,* 79.

[23] Sasaki, T.; Watanabe, M.; Hashizume, H.; Yamada, H.; Nakazawa, H. *J. Am. Chem. Soc.*, **1996,** *118,* 8329.

[24] Sasaki, T.; Watanabe, M. *J. Am. Chem. Soc.*, **1998,** *120,* 4682.

[25] Nakazawa, H.; Yamada, H.; Fujita, T. *Appl Clays Sci*, **1992,** *6,* 395.

[26] Yamada, H.; Nakazawa, H.; Hashizume, H.; Shimomura, S.; Watanabe, T. *Clays Clay Miner,* **1994,** *42,* 77.

[27] Scollenberger, C.DJ.; Simon, R. N. *Clays Clay Miner.* **1946,** *59,* 13.

[28] Hashizume, H.; Shimomura, S.; Yamada, H.; Fujita, T.; Nakazawa, H.; Akutsu, O. *Powder Diffraction* . **1996,** *11,* 288.

[29] Fukushima, Y. *Surfactants in Solution.* **1986,** *6,* 1697.

[30] Toraya, H.; Iwai, S.; Marumo, F. *Z. Kryst.* **1977,** *146,* 73.

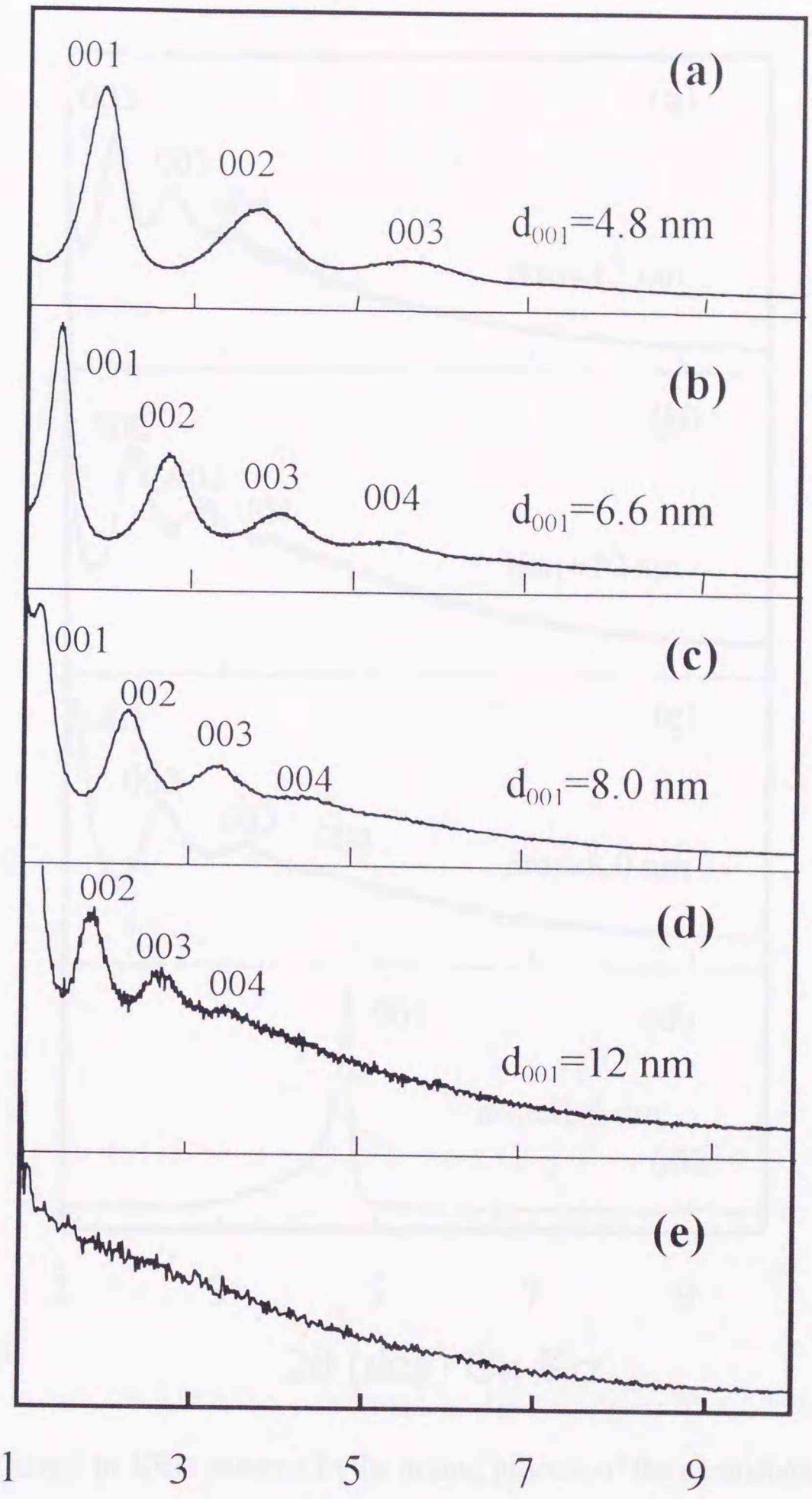

Figure 3.1 Typical XRD patterns for Li-TN aqueous suspensions containing various amounts of water : (a) a weight ratio [H_20] / [Li-TN] of 1.4, (b) 2.6, (c) 4.5, (d) 6.7 and (e) 8.9.

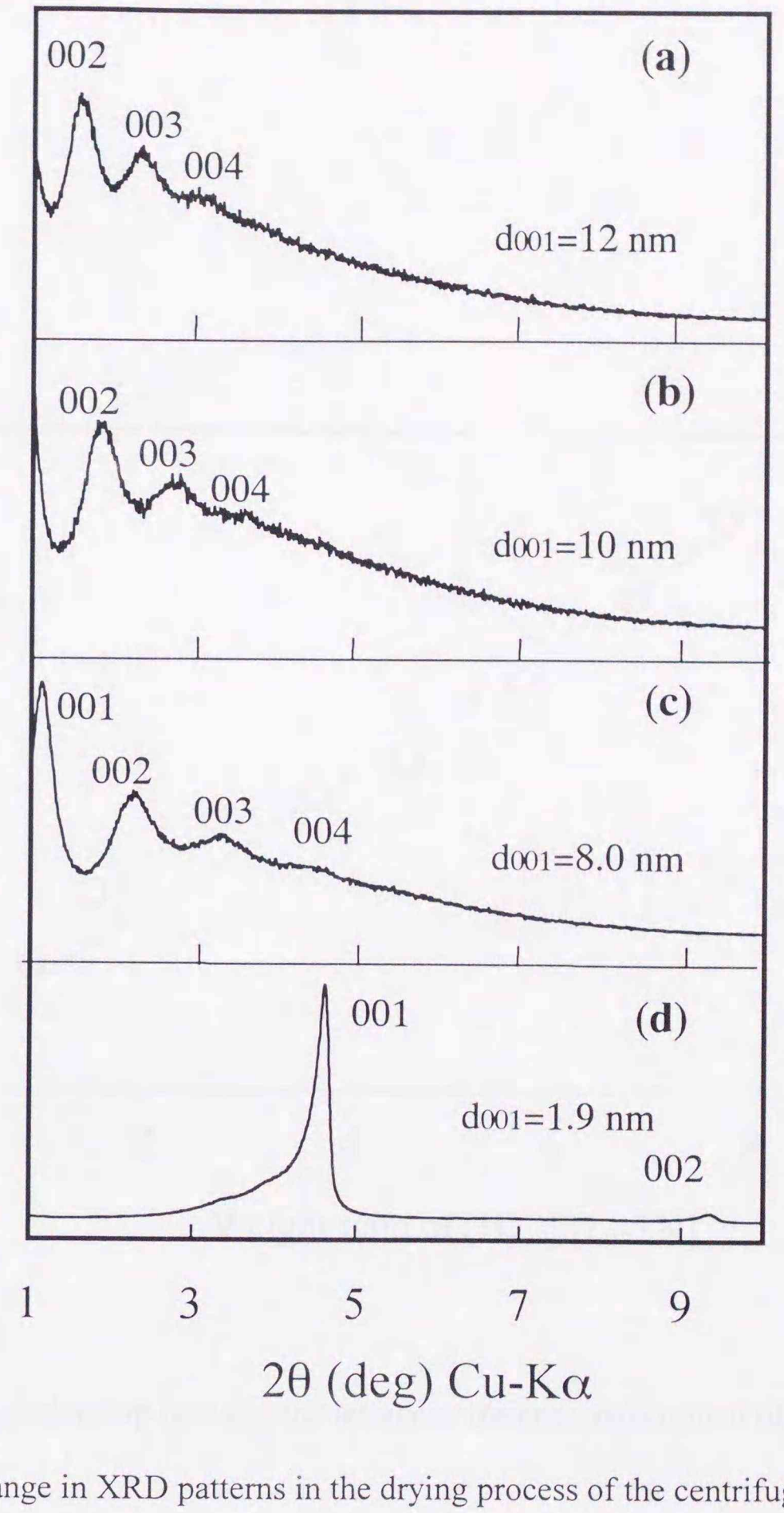

Figure 3.2 Change in XRD patterns in the drying process of the centrifuged sample: (a) Immediately after separation from the liquid phase, (b) conditioned at a relative humidity of 90 % for 1.2 hours, (c) conditioned at a relative humidity of 90 % for 2.7 hours and (d) air dried sample. The intensity scale in (d) is 10 times that in (a). Temperature was regulated at 30 °C and relative humidity was 90 %.

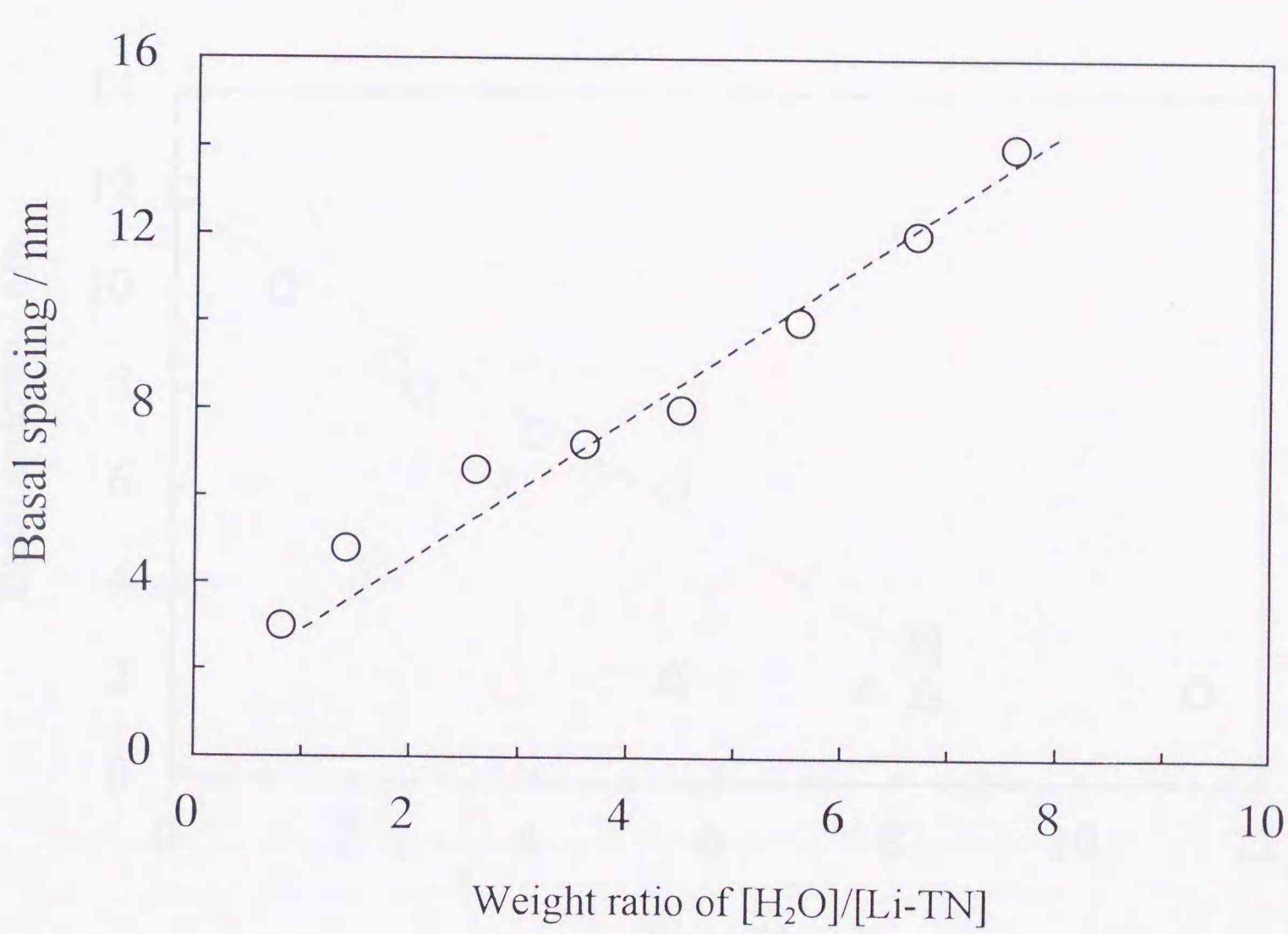

Figure 3.3 Relationship between the interlayer distance and content of suspensions.

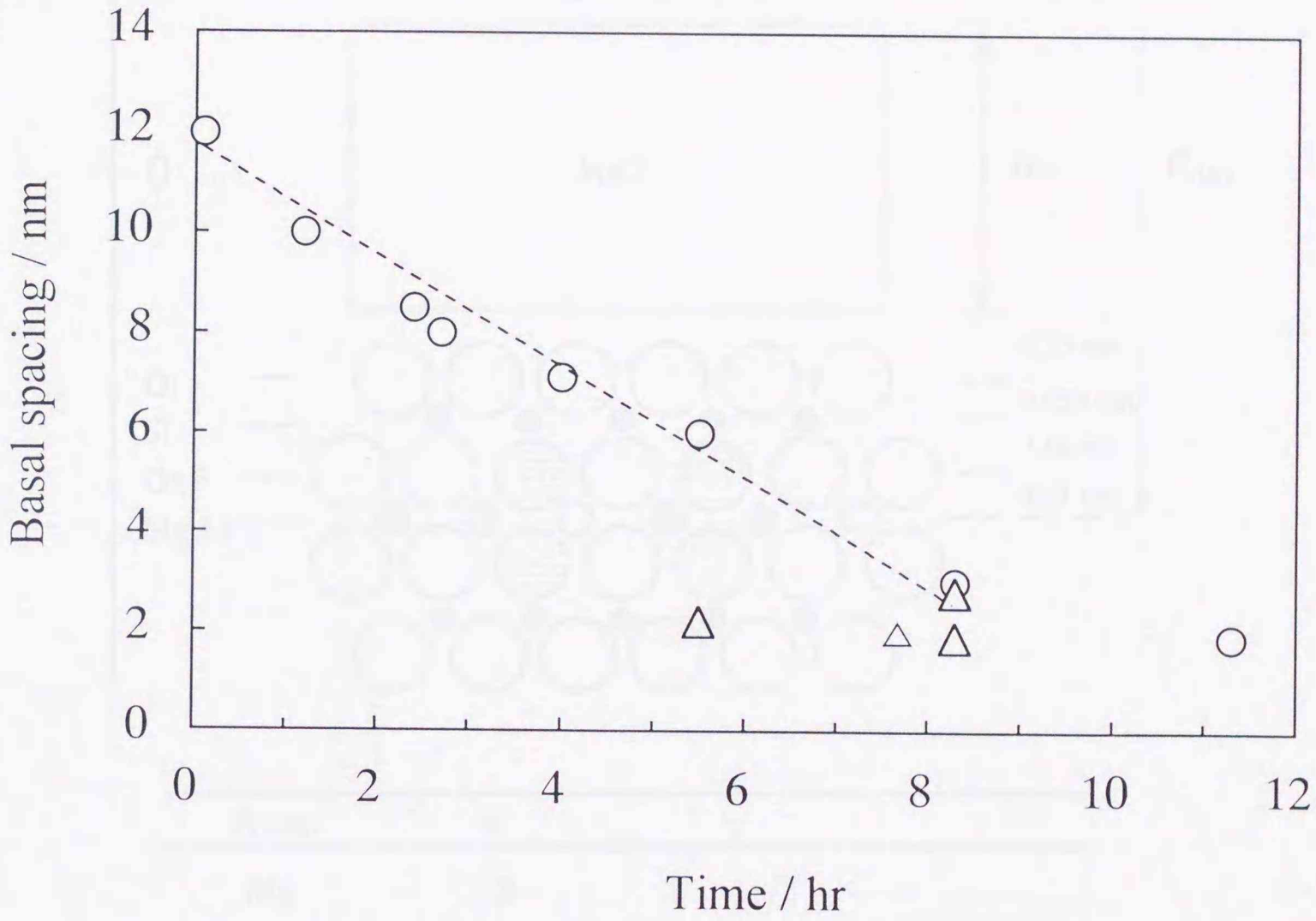

Figure 3.4 Time dependence of the interlayer distance at a constant relative humidity of 90%.

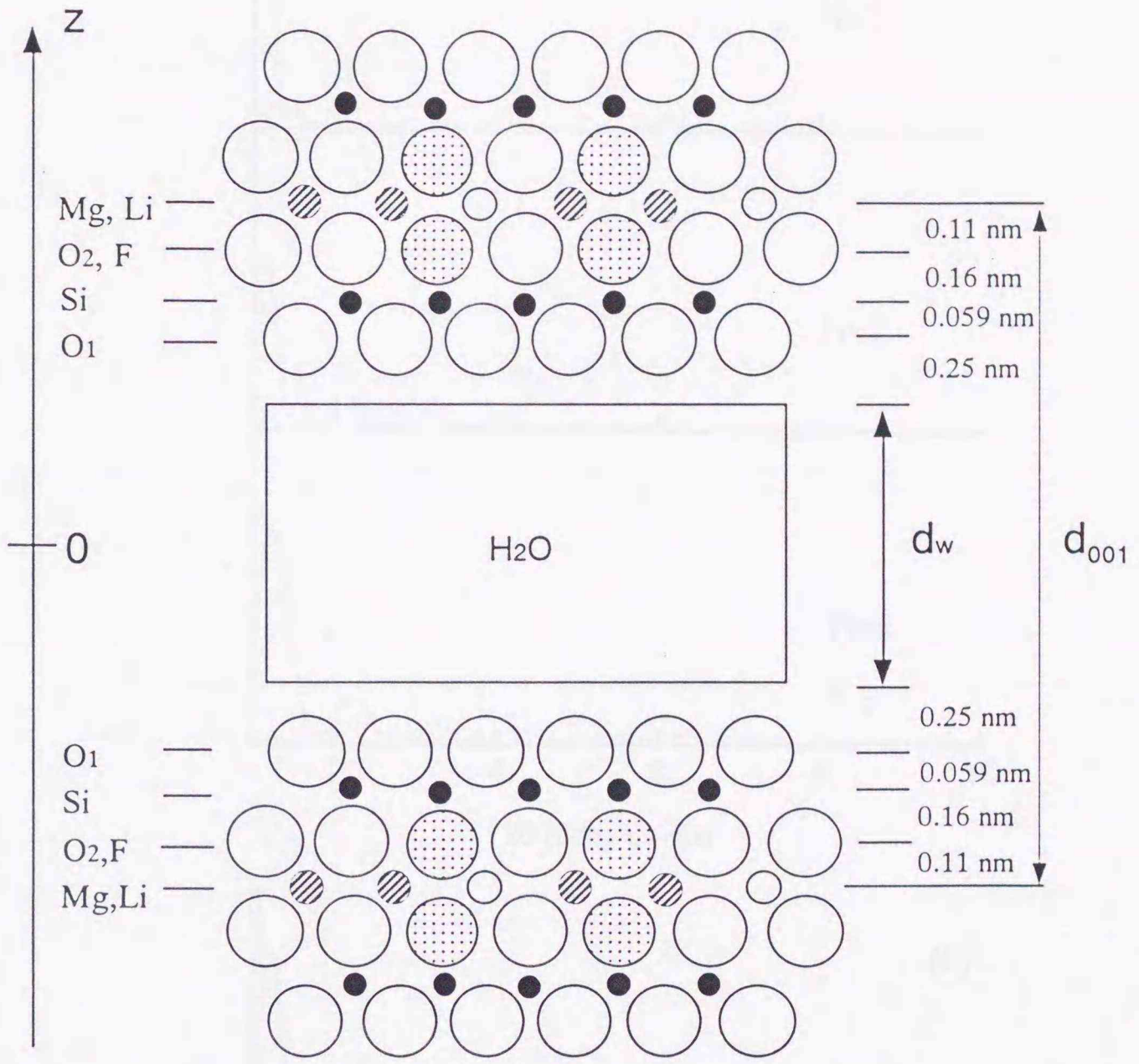

Atom	n	y
Mg	2	± d001/2
Li	1	± d001/2
O1	4	± d001/2-0.11
F	2	± d001/2-0.11
Si	4	± d001/2-0.27
O2	6	± d001/2-0.33
H2O	dw/0.623	-dw/2~+dw/2 (continuous)

Figure 3.5 Structural model for the highly swollen Li-TN. Positional parameters are listed at the bottom.

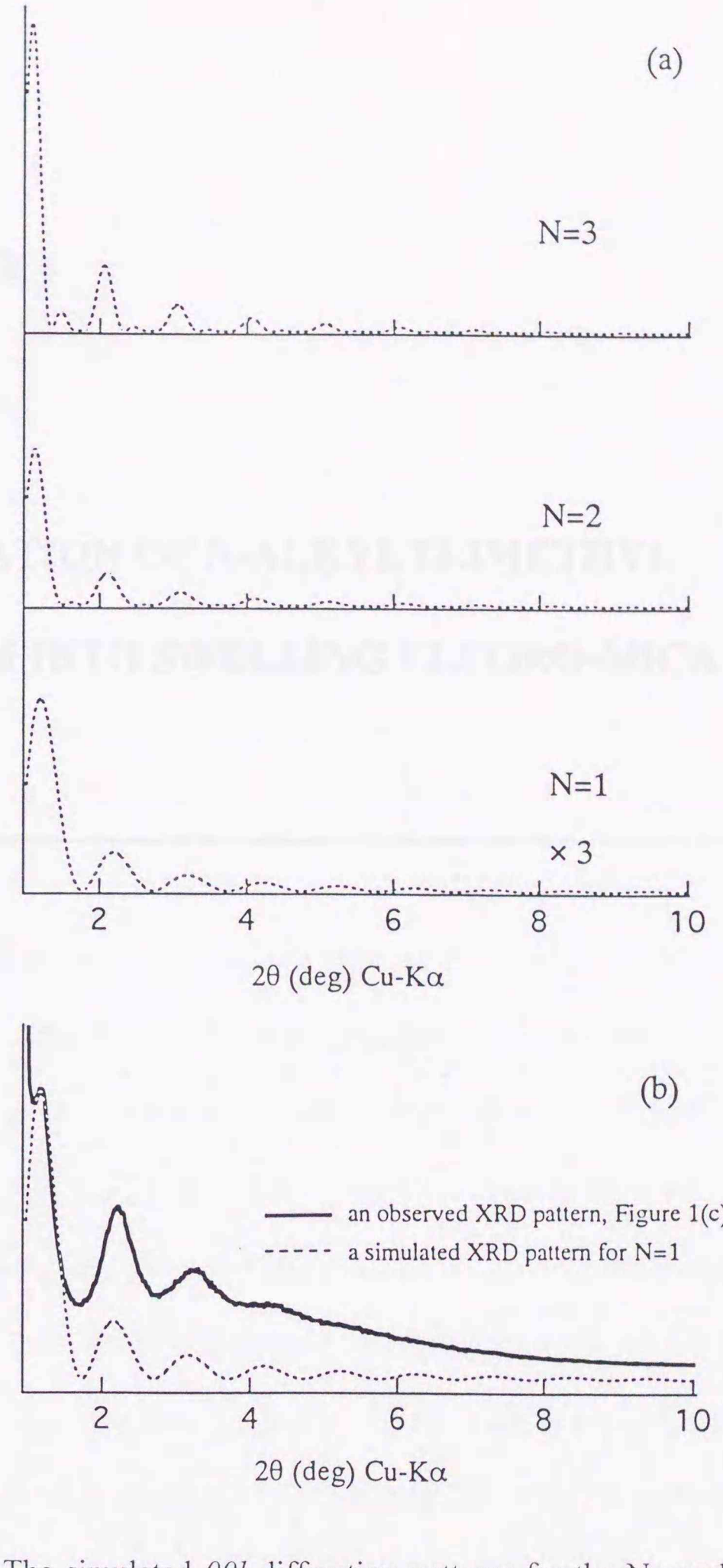

Figure 3.6 (a) The simulated *00l* diffraction patterns for the N parallel sheets with the spacing of 8.0 nm: N=1, N=2, and N=3. (b) Comparison of the diffraction patterns between the experimental data and the simulated line profile. Solid line indicate the XRD pattern at a weight ratio [H_20] / [Li-TN] of 4.5, and dotted line is simulated line profile for N=1, d(001)=8.0 nm.

CHAPTER 4

INTERCALATION OF N-ALKYLTRIMETHYL AMMONIUM INTO SWELLING FLUORO-MICA

ABSTRACT

Trimethylammonium ions (TMA^+) with formula $CH_3(CH_2)_{n-1}N^+(CH_3)_3$, n = 4, 8, 12, 16, 18, 22 were intercalated into synthetic Li-fluorotaeniolite (Li-TN) and Li-fluorohectorite (Li-HT) by cation exchange. The products were analyzed by thermogravimetric (TGA) and X-ray powder diffraction (XRD). XRD patterns exhibited variable (001) spacings of the TMA^+/mica complexes depending on the exchange ratio of TMA^+/ Li^+ and on the carbon number of TMA^+. Detailed inspection of these XRD patterns clarified the structures of the complexes and also the intercalation mechanism, as follows : The fundamental structure of the complexes is the commonly known intercalation structure where the "paraffin-type bilayers" of TMA^+ are in the mica interlayer and their long chains incline at about 30° to the silicate sheet. This structure appeared at the final stage of intercalation reaction. In the intermediate stage of the reaction, units of this structure and those of hydrated mica formed randomly and regularly interstratified structures. Variable (001) spacings in XRD patterns showed the structural change of the complex with increasing number of TMA^+-intercalated units.

4.1 Introduction

Organo-clay complexes have found applications for various fields. For example, reinforced plastics, rheological control agents and chemical sensors.[1]-[5] Their properties depend on the properties of the intercalated organic molecules but also strongly on the physiochemical nature of the host crystals. These studies used natural clays as host crystals and investigated the structure of the complexes, adsorption of organic molecules and others.[6,7] However, the natural clays have properties that have to be interpreted as being due to inhomogeneous inter- and intra-charge distribution and impurity of materials. A well-known text book of clay mineralogy describes the inhomogeneous nature as "the rule with natural montmorillonite".[8] The uncontrollable nature of natural clays results the broad characters of organo-clay complexes.

Recently, fluoro-micas have been synthesized and used on an industrial scale. Some of them, for example fluoro-taeniolite and fluoro-tetrasilicic-mica, are swollen with water in a similar manner to smectites, having interlayer charge densities higher than that of smectites. Unlike natural clays, these have high crystallinity, controllable composition and less impurities. Use of such micas as host materials is therefore expected to be more advantageous than use of natural clays. There have, however, been few studies on the intercalation chemistry of synthetic fluoromicas.

In the present study, quarternary ammonium (n-alkyltrimethylammonium chlorides, TMA) with a variable chain length are intercalated into synthetic fluoro-

taeniolite and hectorite. To observe the intercalation process, the intercalation experiments are performed under controlled exchange ratio. The structures of the organo-mica complexes and the intercalation process are discussed on the basis of XRD observations.

4.2 Experimental

Sample Preparation

The synthetic micas used are commercial fluoro-taeniolite (Li-TN) and fluoro-hectorite (Li-HT) with the ideal formulae of $Li^{+}(Mg_2Li)Si_4O_{10}F_2$ and $Li^{+}_{0.33}(Mg_{2.67}Li_{0.33})Si_4O_{10}F_2$, respectively (Topy Industries Co.,Ltd.). The cation exchange capacities (CEC) of the Li-TN and the Li-HT are 215 meq/100g and 58 meq /100g, respectively (Analysis by Ca adsorption method, Topy Industries Co.,Ltd). The TMA used for cation exchange reaction had formula $[CH_3(CH_2)_{n-1}N(CH_3)_3]^{+}Cl^{-}$, n=4, 8, 12, 16, 18, 22 (NOF Co., Ltd.). A fine powder of the fluoro-micas was stirred with an aqueous solution of the respective ammonium chloride at 60°C for 6 hours. In order to control the exchange ratio the concentration of TMA was varied as 0.5, 1.0, 2.0 of the TMA^{+}/Li^{+} ratio, i.e. the TMA concentrations are half of, equal to and two times the CEC of micas. The solid phase was separated from the suspension by centrifugation at 15000 rpm for 10 minutes. Free trimethylammonium ions were removed by washing with diionized water three times. Finally the solid phase was lyophylized in vacuo($<10^{-2}$ torr) .

Thermogravimetry (TGA)

Thermogravimetric measurements were carried out in the range 30°C to 1000°C in air (TAS-200, RIGAKU). The weight of TMA intercalated in mica was estimated from the total weight loss of thermogravimetric analysis (TGA) in the range from about 150 °C to 1000 °C. Samples (approximately 7 mg) were loaded into platinum crucibles in a dry atmosphere and the sample chamber was heated at 10 °C/min in air.

X-ray powder diffraction (XRD)

The XRD data of the samples were collected in the range between 1.5° and 65° in 2θ at scanning speed of 1.0°/min using a powder X-ray diffractometer with Ni-filtered Cu-Kα radiation (RINT 2000, RIGAKU). The relative humidity was fixed at 10% and temperature at 30°C.

4.3 Results

All TMA having different alkylchain lengths formed intercalation complexes with Li-TN and Li-HT by a cation exchange reaction between TMA^+ and Li^+. The exchange ratio was calculated from the amounts of intercalated TMA^+, obtained by TGA data, and the amounts of exchangable Li^+ in fluoro micas (CEC). They are summarized in Table 4.1. The exchange ratios observed were in the range from about 0.3 to 0.7. Although the intercalation experiments were performed carefully under mild conditions,

as suggested by previous papers, the exchange ratios between Li^+ and TMA^+ were somewhat scattered for the different combinations of TMA and mica samples. [9].

XRD observation

XRD data of the intercalation products show that their basal spacings are expanded to much longer than 0.96 nm, the basal spacing of anhydrous Li-TN and Li-HT, indicating that TMAs intercalate into the micas. The XRD patterns of intercalation complexes of Li-TN and Li-HT with TMAs of different alkylchain lengths are essentially all similar to each other except for their interlayer distances. Typical XRD patterns are presented for the Li-TN/docosyltrimethylammonium(C-22) complexes and for Li-HT/octadecyltrimethylammonium (C-18) complexes in Figure 4.1.a and 4.1.b, respectively. The XRD patterns of the samples treated with different TMA concentrations of 0.5, 1.0 and 2.0 times the TMA^+ / Li^+ ratio are noted as curve 1, curve 2 and curve 3 in Figure 4.1, respectively.

The three XRD patterns of the complexes seem to differ significantly from each other despite their compositional similarity (Fig.4.1.a and 4.1.b). XRD peaks observed in Figure 4.1.a are at 3.98, 3.09, 2.00, 1.55 and 1.34 nm. In them, the reflection at 2.0, 1.55 nm corresponds to (002) of the peak at 3.98 and 3.1 nm, respectively. The others can not be easily assigned. Moreover, some other TMA^+ /TN complexes with TMA^+ of n=16, 12 and 8 showed weak XRD peaks at extremely large spacing. Their profiles and dependence on the exchange ratio of TMA^+ / Li^+ are similar to those at 5.3 nm seen in Fig.4.1.b.

For understanding the interrelations between the complicated XRD patterns, there

is, however, some suggestive behavior in the XRD patterns as the TMA^+ concentration varies. The peaks in curve 1 are broader than those in curve 3. The full width at half maximum intensity (FWHM) of the former peak is about one and a half times greater than that of the latter. Curve 2 appears to be intermediate between curve 1 and curve 3, showing the progress of the intercalation reaction.

All spacings observed for the TMA^+/FTN and TMA^+/HT complexes are plotted against carbon number of alkylchain in Figure 4.2.a and 4.2.b, respectively. Solid symbols indicate the largest spacings of XRD peaks observed for the samples treated with excess TMA (TMA^+/ Li^+=2.0). Examples of these can be seen for the main peaks at 3.98 nm (Figure 4.1.a, curve 3) and at 3.6 nm (Figure 4.1.b, curve 3). Open symbols indicate all other spacings observed. They are calculated from 2θ at half-width of each reflection. For both complexes, there are three linear relations between the basal spacings and carbon number in the range from C=8 to 22 (Fig.2-a and b). In them, the minimum d-spacing at about 1.3 nm does not change with carbon number (line **M**). The extremely long spacings appearing in the complexes treated with lower concentrations of TMA form a linear row with increase of carbon number of TMA (line **O**). The rows of solid symbols, which are the d-spacings of the main reflections, also have linear dependence on the carbon number (line $\mathbf{D_{max}}$). The variations of the interlayer spacing shown by the lines indicate clearly the state of intercalation and the process involved, as discussed later.

4.4 Discussion

As seen in X-ray diffraction patterns (Figure 4.1), the TMA intercalation phenomena of synthetic fluoro-micas are similar to but much clearer than those of natural clays. The micas and TMA formed several complexes of different interstratification depending on maturity of the intercalation reaction. The identification of the phases which appeared and the intercalation mechanism will be discussed below.

The observed phases : Regularly and randomly interstratified organo/fluoro mica complexes. Four phases were identified in the intercalation complexes by interpreting the XRD patterns described above. They are called here $\mathbf{D_{max}}$, **D**, **O** and **M** phases. Phase Dmax is the main phase appearing in the complexes formed by the treatment at highest TMA^+ concentration of 2.0. The XRD peak intensities of the other phases all decreased with increasing TMA^+ concentration (Figure 4.1.a and 4.1.b). The $\mathbf{D_{max}}$ phase is thus the final state of the intercalation whereas the other phases are stable only in the initial or intermediate stages of intercalation. The phase **M** is not a phase of the organo-mica complex but corresponds to hydrated mica, which was deduced from its d-spacing of about 1.3 nm independent of the variable chain length of TMA treated. The **O** phase is a phase stable only in the intermediate stage of intercalation reaction and has an interlayer spacing equal to the sum of those of the $\mathbf{D_{max}}$ and **M** phases, indicating the regular interstratification of the two unit layers. The **D** phase is interpreted as having random stratification of unit layers of the phases $\mathbf{D_{max}}$ and **M**. The continuously

variable d-spacings of the **D** phase are due to variation in the number of the layers intercalated by TMA^+.

HT and TN exhibit quite similar intercalation behavior. However, the intercalation of HT is more sluggish and heterogeneous than that of TN, which is similar to that of natural clay. This is deduced from the observations that 1) the **O** phase appears often with treatment at the highest TMA^+ concentration of 2.0 and 2) the XRD peaks of the TMA/HT composites are broader than those of Li-TN, especially for those treated at low TMA^+/Li^+ ratio (Figure 4.1.a and 4.1.b). Moreover, the TMA/HT complexes showed many more **D** phase peaks in the XRD pattern than do the TMA/TN complexes (Figure 4.2.a and 4.2.b). These differences in the intercalation behaviors of Li-TN and Li-HT are probably due to the differences in crystallinity and homogeneity of charge distribution of the host materials.

Alkylchain arrangements in the interlayers of mica

Alkylchain arrangements in the mica interlayers are reasonably modeled for the $\mathbf{D_{max}}$ phase using the observed d-spacings and some simple assumptions that the alkylchain is in the straight form and has minimum contact with neighboring molecules: a paraffin-type bilayer structure with long chains inclined at about 30° to the silicate sheet. The model for the C-18 TMA/mica complex is shown in Figure 4.3. The angle of chain inclination is calculated from the slope of the d-spacing vs alkylchain carbon number (Figure 4.2.a and 4.2.b). This is the final structure of TMA intercalation reaction into micas. The Li-TN forms this structure in the range of carbon number from C-12 to C-22 and Li-HT in the range from C-18 to C-22. The **O** phase and the **D**

phase are regularly and randomly interstratified structures of unit layers of the **M** and the $\mathbf{D_{max}}$ phases. The **M** phase is the hydrated mica having a layer of water molecules in the interlayer, and is, thus, empty for TMA. The models explain well the linear dependency of the d-values on the carbon number of TMA and the intercalation process as discussed below.

The Intercalation process of TMA into micas

The XRD patterns of the intercalation complexes showed obvious change depending on the TMA^+/Li^+ ratio treated (Figure 4.1.a and 4.1.b). The change in those patterns shows the intercalation process of TMA into micas, which may be explained visually by using the intercalation models mentioned above.

The **O** and the **D** phases are dominant at the intermediate stage of intercalation reaction, and the $\mathbf{D_{max}}$ phase appears finally as the stable state. This indicates that TMA intercalates into the mica interlayer as a unit layer of the $\mathbf{D_{max}}$ structure (Figure 4.3). The layers interstratify with the empty unit layers of the **M** phase partially regularly (the **O** phase) and partially randomly, adjusting the composition of the complex to that of the TMA^+/Li^+ ratio (the **D** phase). As the number of TMA-intercalated layers is increased, the latter converts gradually to the $\mathbf{D_{max}}$ phase and the former phase disappears.

Comparison with previous models

A previous study on n-alkylammonium intercalation to vermiculites concluded that alkylchains oriented at $55° \pm 5°$ to the silicate sheet in the interlayer and the variable

interlayer spacing observed was attributed to some artifacts introduced during the washing and drying process.[10] On the other hand, a recent study by Fourier transform infrared spectroscopy (FTIR) of the alkyl chains intercalated in montmorillonite and fluoro-hectorite indicated that the chains are flexible and assume solid, liquid or liquid-crystal states depending on the interlayer packing density, temperature and chain length.[11] These studies may be helpful for interpretation of variable XRD patterns. However, no attention had been paid in the previous studies to the intercalation process. In the present study, the variable XRD peaks observed have reasonably been interpreted as the phases appearing in the maturation process of the intercalation reaction. The regularly and randomly interstratified structures found in the present work are key structures for explanation of the intercalation mechanism of TMA into micas and the variety of XRD patterns of the complexes.

4.5 Conclusion

Li-TN and Li-HT form intercalation complexes with TMA having different chain lengths. With increasing exchange ratio of TMA^+/Li^+ the complexes initially take regularly and randomly interstratified structures with layer units of TMA and water intercalated layers. Finally, the complexes take a "paraffin-type bilayer structure", where the long chain of TMA inclines at about 30° to the silicate sheet. Li-HT and Li-TN showed quite similar intercalation characteristics, but Li-TN is the better host as demonstrated by the narrower FWHM of the (001) reflections and by the sharper

transition from the regularly and randomly interstratified complexes to the final structure. The difference can predominantly be attributed to higher layer charge and crystallinity of Li-TN.

Acknowledgments

The authors are grateful to Dr. T. Fujita, NIRIM., for his experimental support throughout this work and to Dr. J. R. Hester, NIRIM., for his English corrections. We thank also Mr. H. Inoue, Showa Denko K.K., for his help in $C_4H_9N^+(CH_3)_3Cl^-$, $C_8H_{17}N^+(CH_3)_3Cl^-$ sample preparation, and Mr. A. Ando, Topy Industries Co. Ltd., for supplying Li-TN and Li-HT samples.

References

[1] Fukushima, Y.; Inagaki, S. *J. Incl. Phenom.* **1987,** 5, 473.

[2] Messersmith, P. B.; Giannelis, E. P. *Chem. Mater.* **1994,** 6, 1719.

[3] Wang, M. S.; Pinnavaia, T. J. *Chem. Mater,* **1994,** 6, 468.

[4] Magaruran, E. D.; Kieke, M. D.; Reichert, W. W.; Chiavoni, A. *NGLI Spokesman,* **1987,** 50, 453.

[5] Yan, Y.; Bein, T. *Chem. Mater.* **1993**, 5, 905.

[6] Lagaly, G.; Weiss, A. 1969.*Determination of the layer charge in mica-type layer silicates. Proceedings of the International Clay Conference,* Heller, L. ed., Tokyo, Japan, 61.

[7] Farmar, V. C.; Mortland, M. M. *J. Phys. Chem.***1965,** 69, 683.

[8] MacEwan, D. M. C.; Wilson, M. J. 1980. "*Crystal Structure of Clay Minerals and their X-ray Identification,*" Brindley, G. W.; Brown, G. eds. London: Mineralogical Society, 197.

[9] Walker, G. F. *Clay Minerals.* **1967,** 7, 129-143.

[10] Johns, W. D.; Sen Gupta, P. K. *Am. Mineral.,* **1967,** 52, 1706.

[11] Vaia, R. V.; Rachel, K. T.; Giannelis, E. P. *Chem. Mater.,* **1994,** 6, 1017.

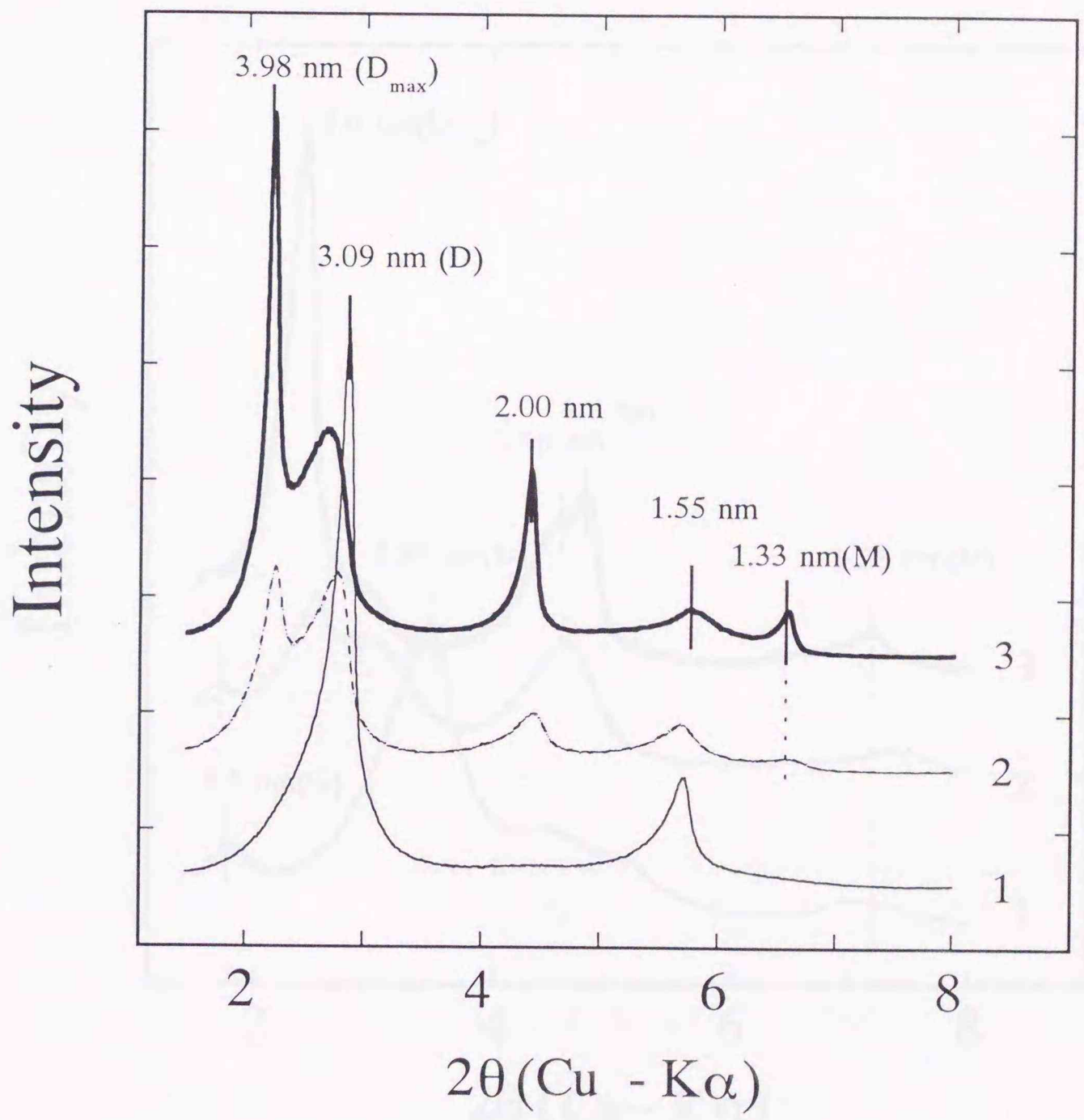

Figure 4.1.a X-ray powder diffraction patterns of mica / TMA complexes : Li-TN / C-22 TMA complexes. The patterns are displaced vertically with added organic content from bottom to top as follows; 0.5, 1.0, 2.0 $[TMA]^+/Li^+$ ratio correspond to curves 1, 2, and 3, respectively.

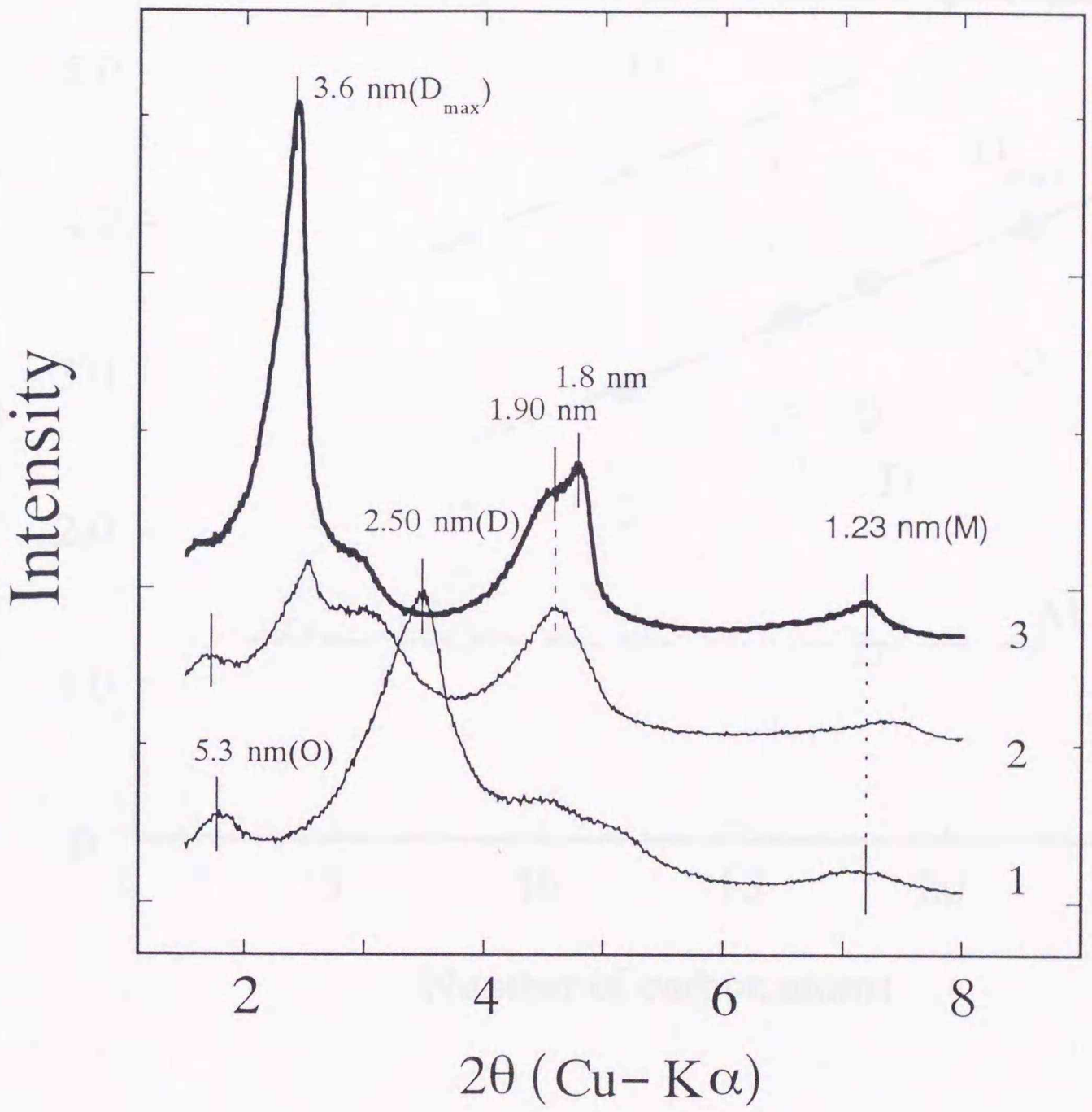

Figure 4.1.b X-ray powder diffraction patterns of mica / TMA complexes : Li-HT / C-18 TMA complexes. The patterns are displaced vertically with added organic content from bottom to top as follows; 0.5, 1.0, 2.0 $[TMA]^+/Li^+$ ratio correspond to curves 1, 2, and 3, respectively.

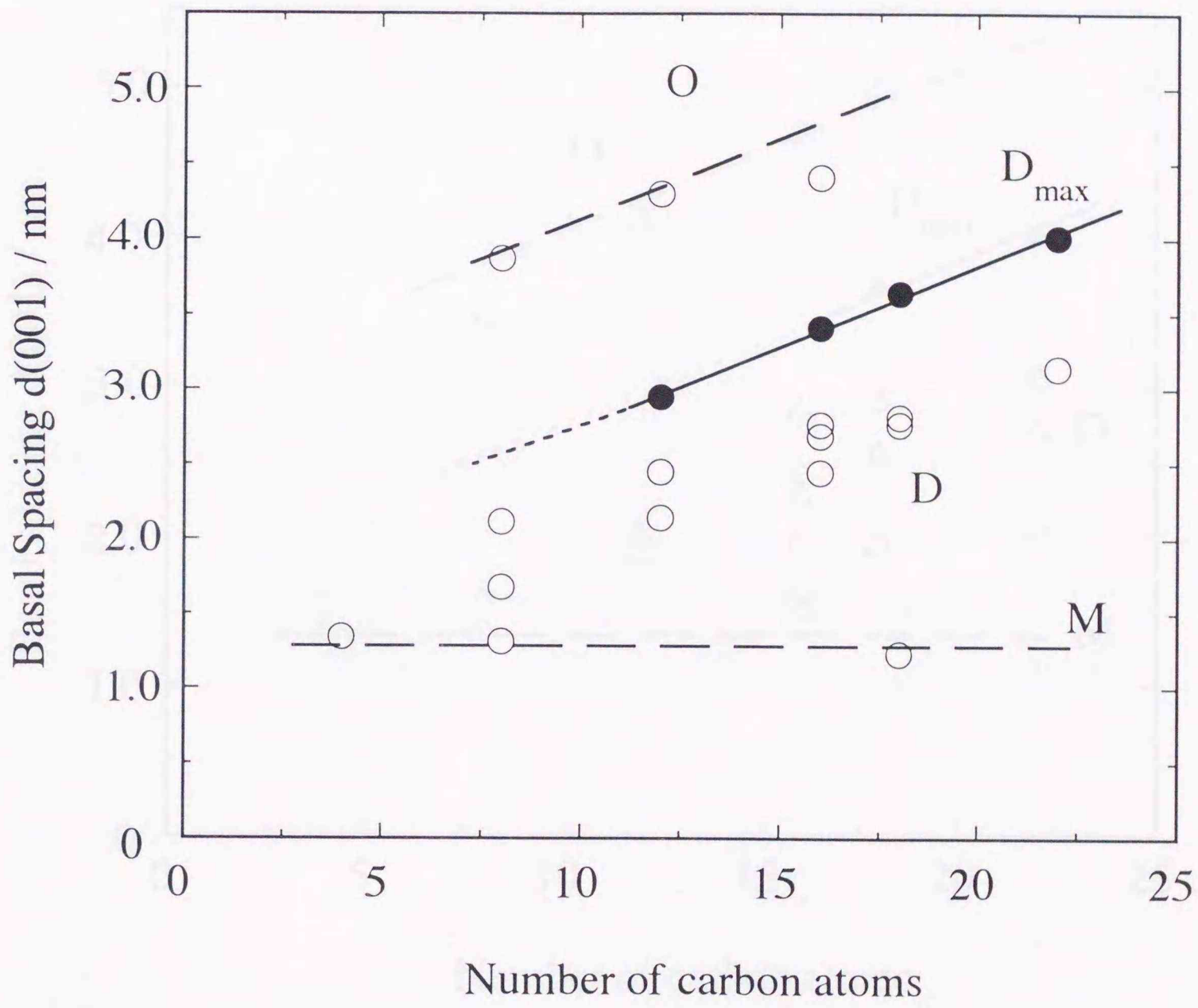

Figure 4.2.a d(001) spacings observed for Li-TN complexes. Solid symbols : Main reflection appeared at the mature stage of intercalation. Open circles : All other peaks appeared.

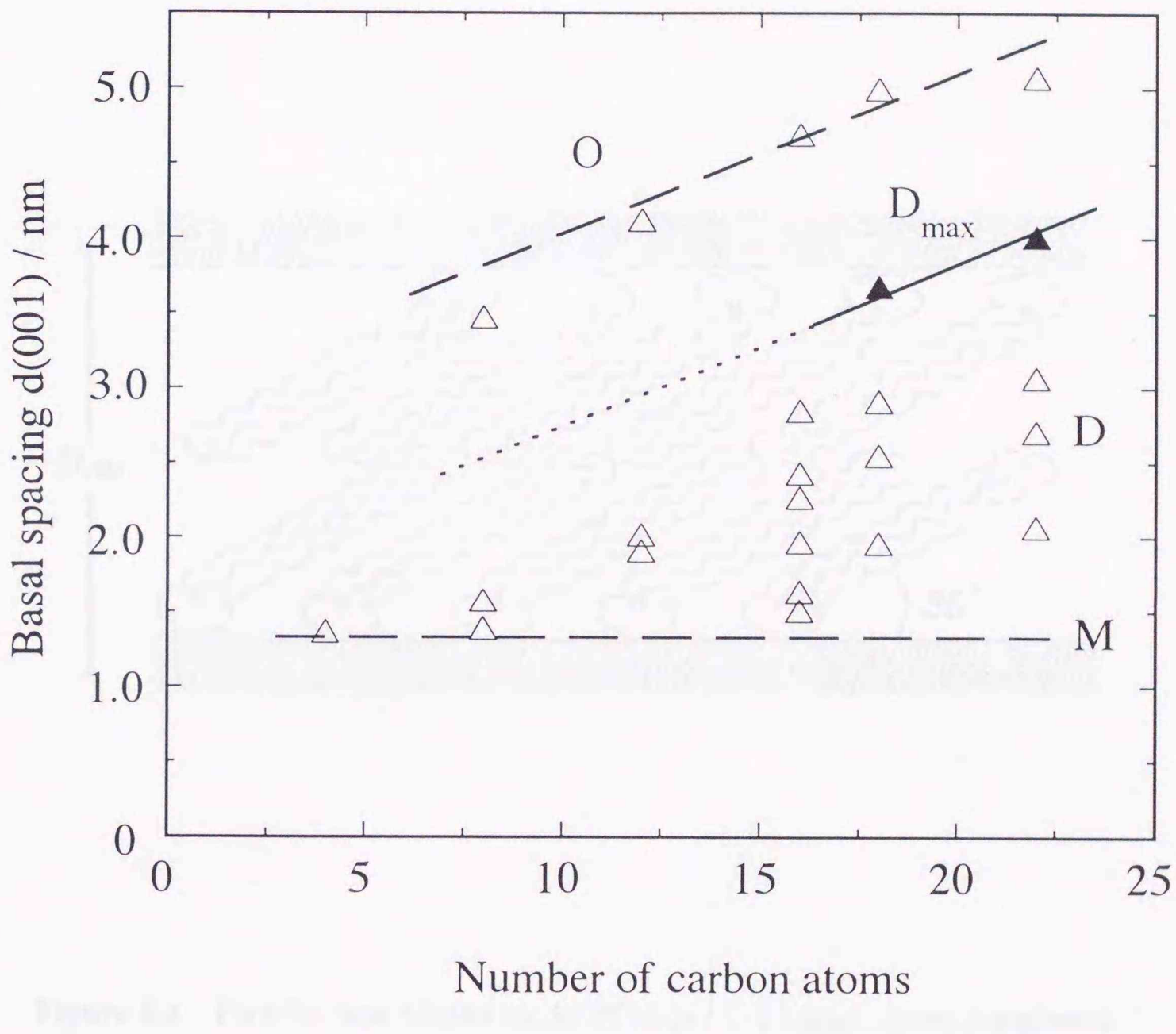

Figure 4.2.b d(001) spacings observed for Li-HT complexes. Solid symbols : Main reflection appeared at the mature stage of intercalation. Open circles : All other peaks appeared.

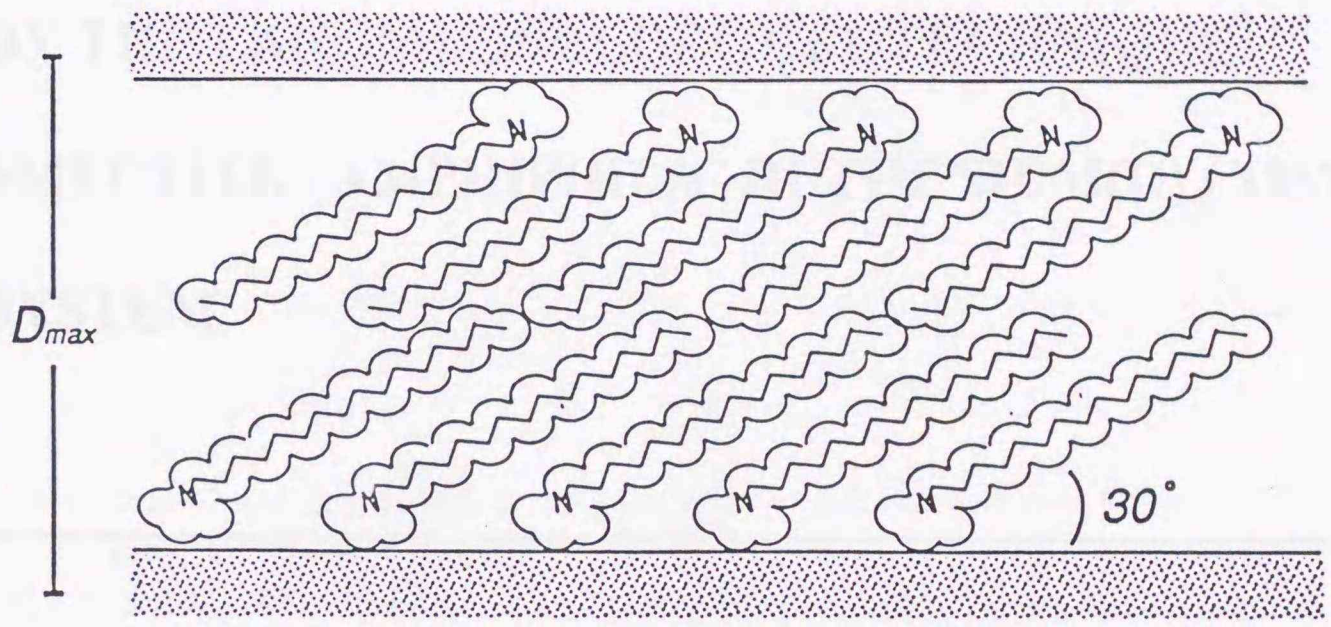

Figure 4.3 Paraffin-type bilayer model of mica / C-18 ammonium complexes.

CHAPTER 5

FORMATION OF LAYER-BY-LAYER COMPOSITE FILM BY THE LANGMUIR-BLODGETT TECHNIQUE: SMECTITE - AMPHIPHILIC RUTHENIUM(II) COMPLEX SYSTEM

ABSTRACT

Organized organic-inorganic ultrathin films have been constructed from the fabrication of smectite unit layers and an amphiphilic ruthenium (II) complex monolayer films using conventional Langmuir-Blodgett (LB) technique. According to the method, a chloroform solution of an amphiphilic ruthenium(II) complex, $[Ru(phen)_2(dC18bpy)]^{2+}$ (phen = phenanthroline, dC18bpy = 4,4'-dioctadecyl-2,2'-bipyridyl as shown in Figure 5.1), was spread onto an aqueous subphase containing exfoliated saponite or hectorite suspension. Brewster angle microscopy (BAM) observation showed that Ru(II) complex molecules formed a self-assembled monolayer on a water surface and that clay particles were adsorbed by the monolayer from an aqueous subphase. A composite film of a Ru(II) complex and clay particle thus formed was transferred onto a hydrophilic glass plate by the vertical dipping method. The surface structure of a deposited film was studied with an atomic force microscope (AFM). As a results, a glass substrate was covered with single sheet of a clay on which an amphiphilic metal complexes were attached.

5.1 Introduction

Construction of organic/inorganic nanostructured materials is an important target of modern materials research. The research has been motivated by a purpose of developing functional materials such as sensors, electrode-modifiers, nonlinear optical devices and pyroelectric materials.[1]-[6] Of particular interest is the preparation of highly ordered organic/inorganic ultra-thin films in which an organic small molecule or a macromolecule is sandwiched between inorganic layers.

One method of preparing such a hybrid film is to attach an inorganic layer onto a self-assembled organic anchor by chemical bond.[7] Another method is to perform layer-by-layer deposition by immersing a solid substrate into a polyelectrolyte solution and an aqueous suspension of inorganic layer compound in an alternative way .[8]

The Langmuir-Blodgett (LB) method has been a well-known technique to prepare a multilayer film from a floating monolayer.[9] A LB film is, however, mechanically weak because the organization of molecules is maintained by van der Waals interactions. To overcome the drawback, we have attempted to construct a hybrid monolayer of a metal complex and a clay particles. In the method, a positively charged monolayer of a metal complex, $[Ru(phen)_2(dC18bpy)]^{2+}$ (phen = phenanthroline, dC18bpy = 4,4'-dioctadecyl-2,2'-bipyridyl as shown in Figure.1), acted as a template for adsorption of a clay particle in a subphase. Here ruthenium(II) polypyridyl complex was selected as an amphiphilic compound since it is known to be an effect converter from light energy to chemical energy.[10] By applying the Langmuir-Blodgett technique to such a

composite film, we have constructed a new organic/inorganic nano-structured film. A film will be able to be used as a functional device for energy converter. This is an extension of our previous works on the preparation of LB films of metal complexes and inorganic layer compounds.[11]-[17]

5.2 Experimental

Materials

An amphiphilic Ru(II) complex, $[Ru(phen)_2(dC18bpy)]^{2+}$, was synthesized by refluxing $Ru(phen)_2Cl_2$ (50 mg) and dC18bpy (70 mg) with $AgNO_3$ (32 mg) in 20 ml of an ethanol solution for 20 min. An orange precipitate was formed by adding $NaClO_4$ to the reactant mixture. Swelling clays used are synthetic saponite (denoted by Sap; Smecton, Kunimine Industries Ltd., Japan) and synthetic lithium hectorite (denoted by Li-HT; Topy Industries Ltd., Japan). The chemical composition and cation exchange capacity (CEC) are stated to be $[(Na_{0.25}Mg_{0.07})[(Mg_{2.98}Al_{0.01})\ (Si_{3.6}Al_{0.4})O_{10}(OH)_2])$ and 80 meq/100g for Sap, and $[Li_{0.6}(Mg_{2.5}Li_{0.6})Si_{3.9}O_{9.8}F_{2.2}])$ and 140 meq/100g for Li-HT, respectively. The average size of Sap was determined to be 0.19 μm in the previous experiment.[18] For Li-HT, the fraction with the 0.6 μm median particle size was separated by sedimentation. and used throughout the study. They were dispersed by being stirred for 1 day in distilled water.

Instruments

Surface pressure-area (π-A) curves were measured with a Langmuir trough (U.S.I., Japan) at 25 °C. Compression of a surface was started 30 minutes after a chloroform solution of a metal complex was spread onto a water surface. The rate of compression was 10 cm^2/min. A LB film was prepared by a vertical dipping method at the dipping rate of 10 mm/min. BAM experiments were performed with an instrument constructed by Dr. H. Yokoyama (Electrotechinical Laboratory, Japan). Reflected light passed through a lens to a CCD camera and the resulting video signal was fed to a video system. The AFM images were recorded at room temperature under air with a Nanoscope III scanning probe microscope (DI Instruments, USA), using Nanoprobe integral cantilevers (Si_3N_4) having tips with a spring contact of 0.06nm^{-1} (Park Scientific). The AFM images were obtained in the tapping mode with filters off. The 'd' scan head was used, which has a maximum scan range of 12 μm by 12 μm by 4.4 μm.

5.3 Results

Surface pressure-molecular area (π-A) isotherm

Curve (a) in Figure 5.2 shows a surface pressure-molecular area (π-A) isotherm when a chloroform solution of $[Ru(phen)_2(dC18bpy)](ClO_4)_2$ was spread on an aqueous 0.1 M $NaClO_4$ solution. The curves were obtained with good reproducibility when the measurements were repeated after 30 minutes. Surface pressure rose from zero at about 1.2 nm^2 per molecule and became nearly constant at 50 mN/m below 0.5 nm^2 per molecule. The critical surface area A_i , which was defined as the surface area where

the straight line intercepted the horizontal axis, was determined to be 1.0 nm^2. The observed lift-off area (1.2 nm^2 per molecule) was nearly equal to the cross sectional area of the head group of the complex (1.5 nm^2 per molecule). The result indicated that the molecule formed closely packed monolayer and collapsed at the surface pressure above 50 mN/m. [17][19]

Curve (b) and (c) show π-A isotherms when chloroform solutions of $[Ru(phen)_2(dC18bpy)](ClO_4)_2$ was spread on aqueous suspension of Sap (0.015g/l) or Li-HT (0.008 g/l), respectively. Curves (b) attained a plateau at 40 mN/m with the critical surface area (A_i) of 1.2 nm^2, while curve (c) attained a plateau at 40 mN/m with the A_i of 1.6 nm^2.

Figure 5.3 shows the effect of a clay concentration on a π-A isotherm. Curve (a) and (b) are the results when a chloroform solution of $[Ru(phen)_2(dC18bpy)](ClO_4)_2$ was spread on aqueous suspensions of 0.015 or 0.050 g/l) suspension of Sap, respectively. Curve (c) and (d) are results when a chloroform solution of the same complex was spread on an aqueous 0.008 or 0.022 g/l suspension of Li-HT, respectively. In both cases, the increase of clay concentration resulted in the increase of critical area (A_i) and the lowering of the collapse pressure (π_c).

Brewster angle microscope (BAM)

Interaction of a clay with a monolayer was studied with a Brewster angle microscope (BAM). A floating bright region was observed when a chloroform solution of $[Ru(phen)_2(dC18bpy)](ClO_4)_2$ was spread on an aqueous $NaClO_4$ solution. It implied that $[Ru(phen)_2(dC18bpy)]^{2+}$ molecules formed monolayer domain already

at zero surface pressure. On compressing a surface, the surface increased brightness until the whole surface became bright at the on-set of surface pressure (Figure 5.4B). At the surface pressure higher than 50 mN/m, a highly intensely bright region appeared as indicated by an arrow, indicating that a monolayer was collapsed to form a multilayer (Figure 5.4C). Since the straight line extended over a few thousand micrometers, the monolayer was thought to be uniform over that region before collapse.

Figure 5.5 shows the BAM results when the same metal complex was spread on an aqueous suspension (0.015 g/l) of Sap. A floating bright region was observed as already seen on an aqueous $NaClO_4$ solution. On compressing a surface, the surface increased brightness until the whole surface became bright at the on-set of surface pressure (Figure 5.5B). At the surface pressure larger than 43 mN/m, an intensely bright region appeared as indicated by arrows, indicating the collapsed to form a multilayer (Figure 5.5C).

Figure 5.6 shows the BAM results when the same metal complex was spread on an aqueous solution (0.010 g/l) of Li-HT. Even at zero surface pressure, bright spot with the radii of 10 - 100 μm appeared on the surface (Figure 5.6A). On compressing a surface, the density of bright spots increased until it covered the whole surface (Figure 5.6B). At the surface pressure larger than 45 mN/m, a bright straight region appeared, indicating the collapse of a film (Figure 5.6C). In this case, the intensely bright region extended in a zigzag way only less than one thousand micrometers.

Atomic force microscope (AFM)

When a hydrophilic glass plate was moved upwards at the rate of 10 mm/min

under the condition of Figure 5.5B and 5.6B, a floating film was transferred with a transfer ratio of about 0.8 at 20 mN/m. The surface structure of a film thus deposited was investigated with an atomic force microscope (AFM). Figure 5.7 show the AFM images of film transferred from aqueous suspension of Sap. A glass plate was covered with a layer of 1 - 2 nm thickness. No clear image, however, of particles was seen except for small high regions of less than 20 nm. This was probably because the adsorbed particles of Sap were packed together so closely.

Figure 5.8A shows the AFM image of a film transferred from an aqueous suspension of Li-HT. A glass plate was covered with planar sheets whose size thickness were estimated to be 0.5 - 10 μm and 1.5 nm, respectively. The thickness of a sheet was close to that of a single clay layer; 1.0 nm.[20] In a different image, sheets were partially overlapped to form a double layer as indicated by an arrow (Figure 5.8B). In that region, the thickness of an upper layer was estimated to be 6 nm, which was close to the sum (4.5 nm) of the molecular height of $[Ru(phen)_2(dC18bpy)]^{2+}$ (3.5 nm) and the thickness of a single layer of hectorite (1.0 nm). Thus the layer was concluded to be a hybrid layer of a metal complex and a clay sheet.

5.4 Discussion

The above results have shown that a monolayer of a cationic amphiphilic metal complex acted as a template for the adsorption of a clay particle in a subphase. As a results, the hybrid film of a metal complex and a clay particle was formed at an air-water

interface and efficiently transferred onto a solid substrate. In this study, two kinds of smectite clays have been used: saponite (Sap), trioctahedral smectite with tetrahedral charge and hectorite (Li-HT), trioctahedral smectite with tetrahedral charge. It has been intended to clarify the effects of size and charge density of a clay layer on the construction of a film. The structure of a hybrid film and its built-up process are discussed on the basis of results from Brewster angle microscope (BAM) and atomic force microscope (AFM) measurements.

According to the results Figure 5.2, isotherm was displaced by 1.0 nm^2 towards the larger molecule area or from A_i=1.0 nm^2 for an aqueous subphase of $NaClO_4$ to 1.2 and A_i=1.8 nm^2 for aqueous suspension of Sap and Li-HT, respectively. The results confirmed the interaction of a clay with a cationic monolayer. A critical area, A_i, corresponded to the area occupied by one metal complex and clay sheet. We calculated the negative charge in a clay layer occupied by one metal complex under that condition. On the basis of the elemental compositions as given in the experimental section, A_i carried the negative charge of -1.0 e and -2.3 e for Sap and Li-HT, respectively. For Li-HT, the value was nearly equal to the positive charge of the metal complex (+2), while it was half of that for Sap. As a results, it was concluded that a metal complex was adsorbed by a clay particle by the ion-exchange mechanism in case of Li-HT, while a metal complex was adsorbed in excess over the cation-exchange capacity of Sap. In the latter case, therefore, external anions were included in a hybrid film to neutralize excess positive charge. The surface pressure in such a film arose from the repulsive interactions among metal complexes but not among clay particles. These results indicated that adsorption mechanisms depended on the types of a clay

remarkably.

Nearly the identical curves were obtained when compression-expansion experiment was repeated on clay suspensions under the above conditions. The results indicated that only one side of a clay sheet always interacted with the cation monolayer of a metal complex although both sides of a clay sheet were identical in a bulk medium.

The formation of ultrathin hybrid film also depended upon the concentration of smectite in subphase. The π-A isotherms in Figure 5.3 show that the increase of clay concentration resulted in the increase of A_i. In other words, the surface density of a metal complex in a hybrid film decreased with the increase of a clay concentration. Such situations would be caused by the aggregation of a clay particle from a subphase at the higher concentration. The formation of parallel stacks of platelets as well as face-to-edge and edge-to-edge agglomerates at an air-water interface.

The BAM observation provided no definite evidence for the adsorption of a Sap particle with a monolayer at an air-water interface. In the case of Li-HT, however, the adsorption was confirmed by the appearance of highly bright spots with the radii of 10 - 100 μm on the surface (Figure 5.5A). No such spots appeared in the absence of a monolayer of $[Ru(phen)_2(dC18bpy)](ClO_4)_2$. High brightness was undoubtedly due to the refractive index of clay layers; 1.53.[20] The formation of a hybrid film was also confirmed by the increase of spot density on compressing a surface (Figure 5.5B).

The AFM results in Figure 5.8 were consistent with a view that the surface was covered with a monolayer of $[Ru(phen)_2(dC18bpy)](ClO_4)_2$ **(b)**, a monolayer of $[Ru(phen)_2(dC18bpy)]^{2+}$ and a hectorite sheet **(a)** and a bilayer of $[Ru(phen)_2(dC18bpy)]^{2+}$ and a hectorite sheet **(c)**. Since there was no double layer

region of clay sheets only observed in the AFM images, it was concluded that no self-stacking of clay sheets took place at least in an interfacial region. Notably double layer region **(c)** were connected smoothly with single layer regions **(a)**, implying that an upper layer was so flexible to change its shape according to the up-and-down of an underneath surface. Figure 5.9 presents a schematic illustration of the AFM image of Figure 5.7C.

5.5 Conclusions

We have investigated the effects of the particle size and charge density of smectite on the formation of LB hybrid thin film. As a result, an ultrathin film was constructed by fixing an amphiphilic ruthenium complex to a rigid inorganic sheet. A clay layer may have a role to enhance the mechanical strength of a film and to fix an adsorbed molecule in two-dimensional regularity. Hybridization is facilitated by electrostatic anchoring of the cationic head group of a metal complex onto the anionic sheet of a clay. Appropriate chose of smectites and amphiphilic compounds allows LB films of uniform thickness to be constructed.

Acknowledgment

We want to thank Prof. T. Nakamura, Associate Prof. T. Hasegawa and Dr. T. Akutagawa (Research Institute for Electronic Science, Hokkaido University), for support brewster angle microscope experiments. We also thank Dr. H.Yokoyama (Electrotechinical Laboratory) for constructing a Brewster angle microscope.

References

[1] Ichinose,I.; Kimizuka,N.; Kunitake,T. *J. Phys.Chem.* **1995,** *99,* 3736-3741.

[2] Kotov,N.A.; Haraszi,T.; Turi,L.; Zavala,G.; Geer,R.E.; Dèkàny,I.; Fendler,J.H. *J. Am. Chem. Soc.,* **1997,** *119,* 6821-6832.

[3] Kotov, N.A.; Dèkàny,I.; Fendler, J.H. *J. Phys. Chem.,* **1995,** *99,* 13065-13071.

[4] Lvov,Y.; Ariga,K.; Ichinose,I.; Kunitake,T. *Langmuir*. **1996,** *12,* 3038-3044.

[5] Swalen, J.D.; Allara, D.L.; Andrade, J.D.; Chandross, E.A.; Garoff,S.; Israelachvili, J.; McCarthy, T.J.; Murray, R.; Pease, R.F.; Rabolt, J.F.; Wynne, K.J.; Yu, H. *Langmuir.* **1987,** *3,* 932-950.

[6] Tsutsumi,N.; Sakata,K.; Kunitake,T. *Chem.Lett.* **1992,** 1465.

[7] Rong, D.; Kim,Y.; Mallouk,T.E. *Inorg. Chem.* **1990,** *29,* 1531-1535.

[8] Kleinfeld, E.R.; Ferguson,G.S. *Science.,* **1994,** *265,* 370-373.

[9] Gaines, G.L.Jr. **1966.** "*Insoluble Monolayers at Liquid-Gas Interfaces*", Interscience Publishes, NY

[10] Rotzinger, F. P.; Munavalli, S.; Comte, P.; Hurst, J. K.; Gratzel, M.; Pern, F.; Franck, A. *J. Am. Chem. Soc.,* **1987,** *109,* 6619-6623.

[11] Aramata, K.; Kamachi, M.; Taniguchi, M.; Yamagishi, A. *Langmuir,* **1997,** *13,* 5161-5167.

[12] Aramata, K.; Kajiwara,A.; Kamachi, M.; Umemura, Y.; A. Yamagishi, *Macromolecules,* **1998,** *31,* 3397-3403.

[13] Inukai, K.; Hotta, Y.; Taniguchi, M.; Tomura, S.; Yamagishi, A. *J. Chem. Soc.,*

Chem. Commun., **1994,** 959.

[14] Hotta, Y.; Taniguchi, M.; Inukai, K.; Yamagishi, A. *Clay Miners.,* **1997,** *32,* 79.

[15] Hotta, Y.; Inukai, K.; Taniguchi, M.; Yamagishi, A. *J. Electroanal. Chem.* **1997,** *429,* 107-114.

[16] Yamagishi, A.; Goto, Y., and Taniguchi, M. (1996) *J. Phys. Chem.* **100,** 1827.

[17]Yamagishi, A., Sasa, N.; Taniguchi, M.; Endo, A.; Sakamoto, M.; Shimizu, K. *Langmuir.* **1997,** *13,* 1689-1694.

[18] Nakamura, Y.; Yamagishi, A.; Iwamoto, T.; Koga, M. *Clays Clay Miner.* **1988,** *36,* 530-536.

[19] Yamagishi, A.; Taniguchi, M.; Takahashi, M.; Asada, C.; Matsushita, N.; Sato, H. *J.Phys.Chem.* **1994,** *98,* 7555.

[20] Sudo,T. **1974.** *"Nenndo Koubutugaku (Clay Minerals)*", Iwanami.

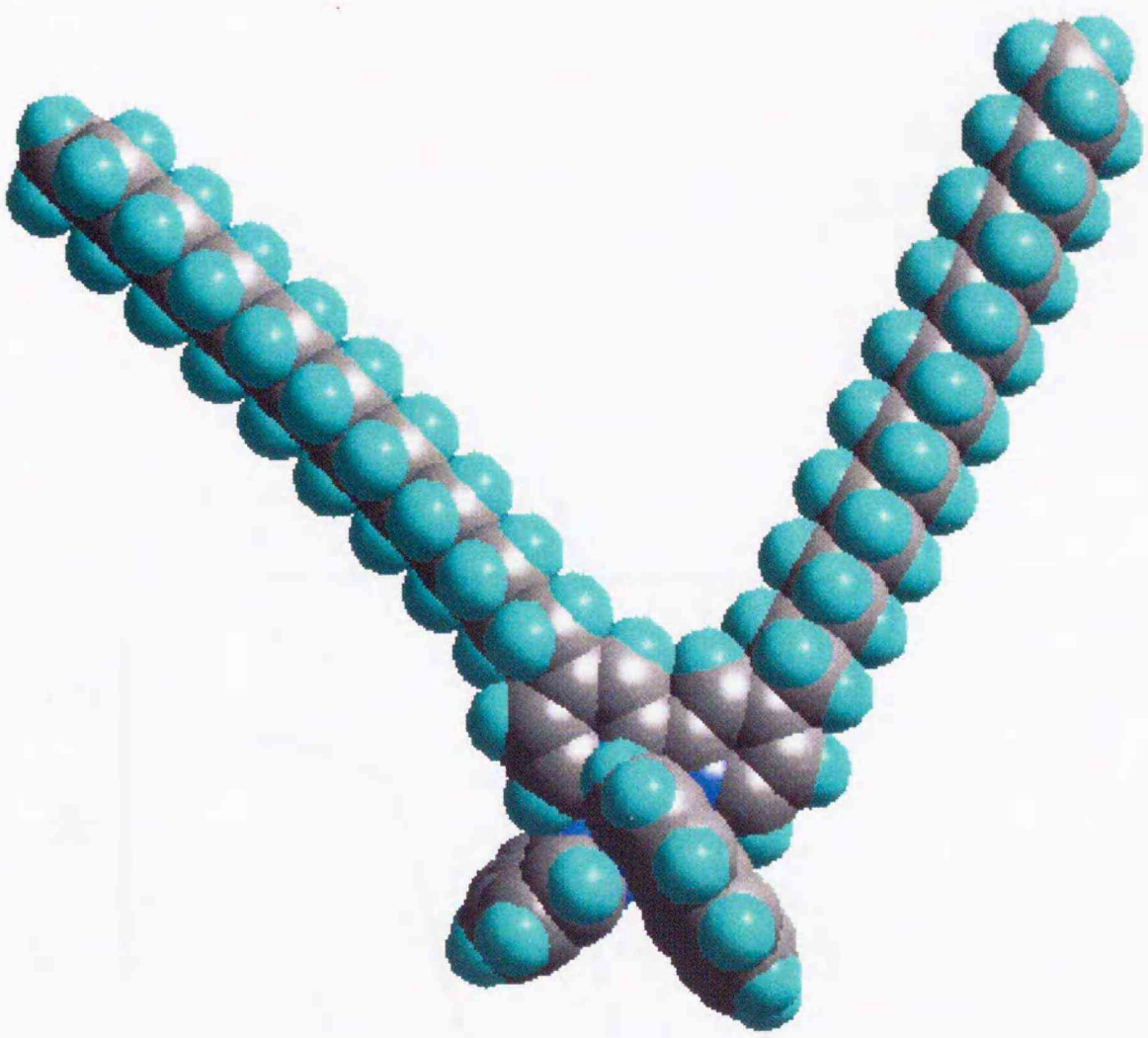

(a) Side view

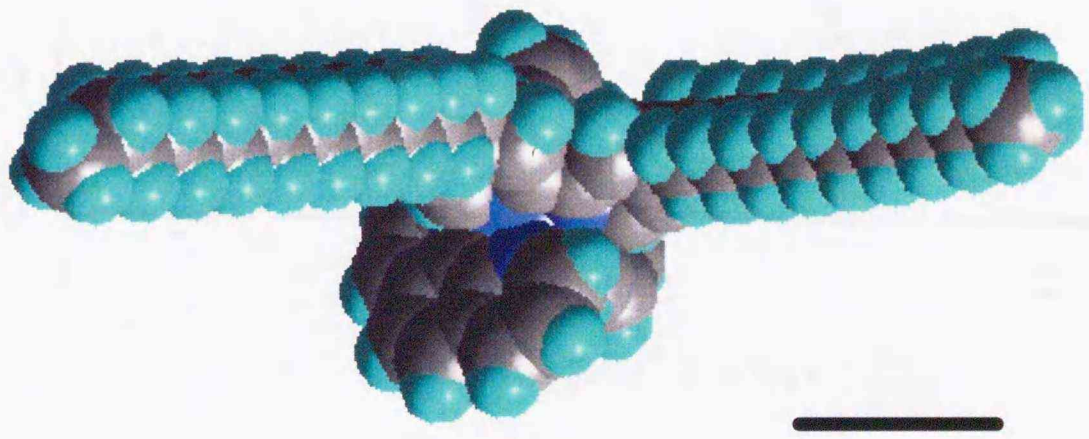

0.5 nm

(b) Top view

Figure 5.1 A molecular model of $[Ru(phen)_2(dC18bpy)]^{2+}$

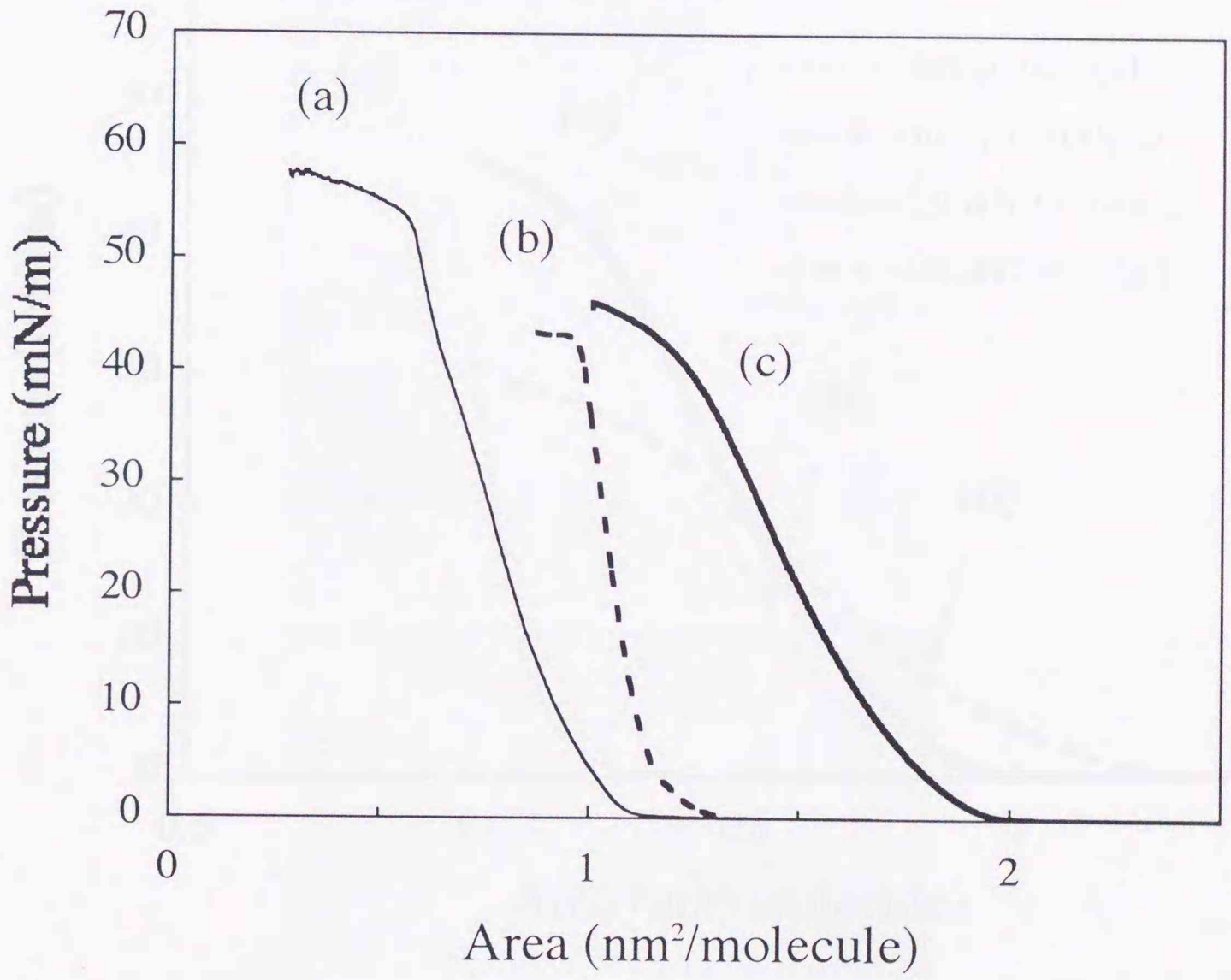

Figure 5.2 Surface pressure-molecular area (π-A) curves at 25°C when a chloroform solution of $[Ru(phen)_2(dC18bpy)](ClO_4)_2$ was spread onto various subphases; (a) 0.1 M $NaClO_4$ aqueous solution, (b) saponite suspension (0.015g/l), and (c) hectorite suspension (0.008 g/l).

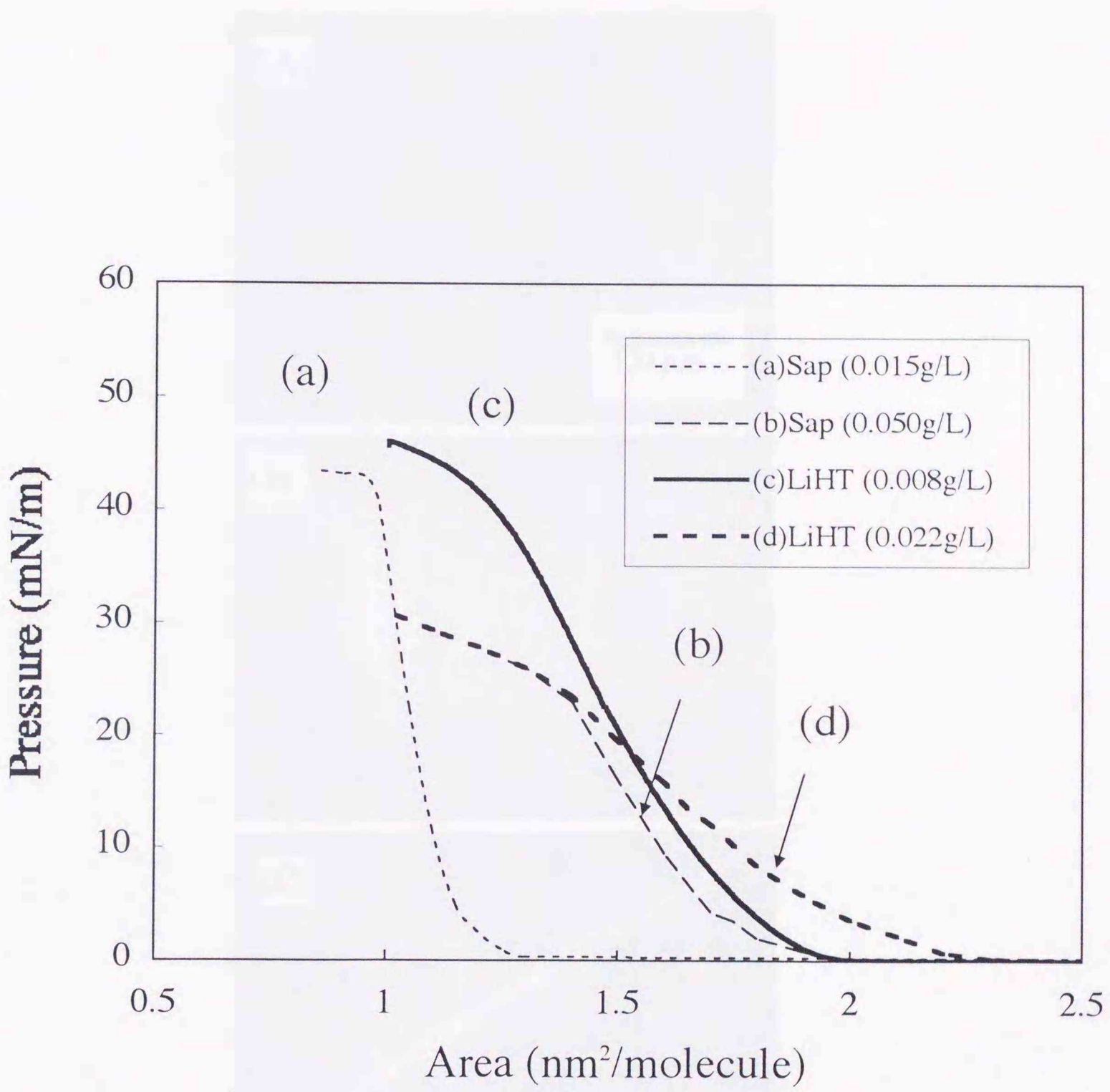

Figure 5.3 Surface pressure-molecular area (π-A) curves at 25°C when a chloroform solution of $[Ru(phen)_2(dC18bpy)](ClO_4)_2$ was spread onto smectite suspensions with different concentrations; (a) saponite suspension (0.015g/l), (b) saponite suspension (0.050 g/l), (c) hectorite suspension (0.008 g/l) and (d) hectorite suspension (0.022 g/l).

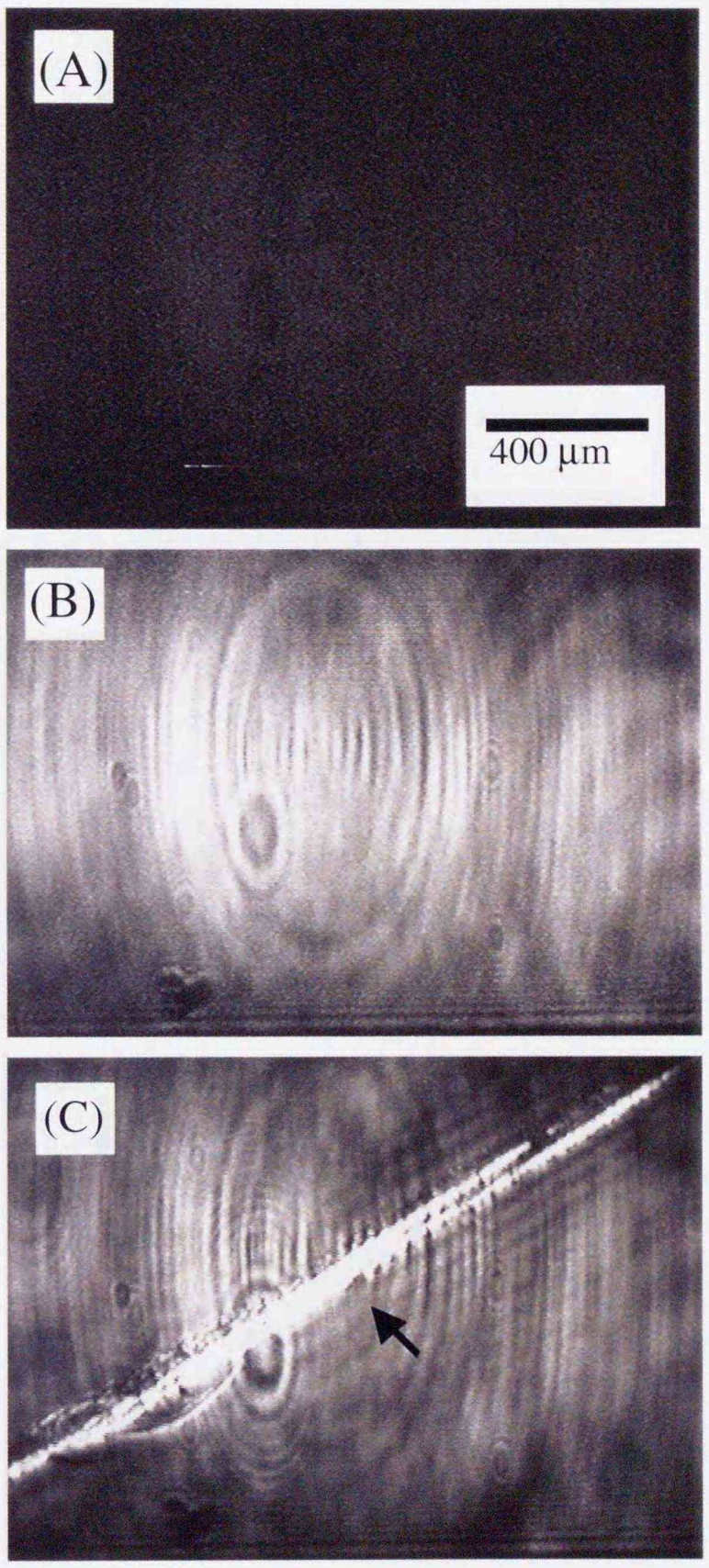

Figure 5.4. Brewster angle microscope images of a trough surface: (**A**) a surface of an aqueous $NaClO_4$ solution; (**B**) a surface compressed to 20 mN/m after a chloroform solution of $[Ru(phen)_2(dC18bpy)]$ $(ClO_4)_2$ was spread onto an aqueous $NaClO_4$ solution; (**C**) the same surface compressed to 50 mN/m.

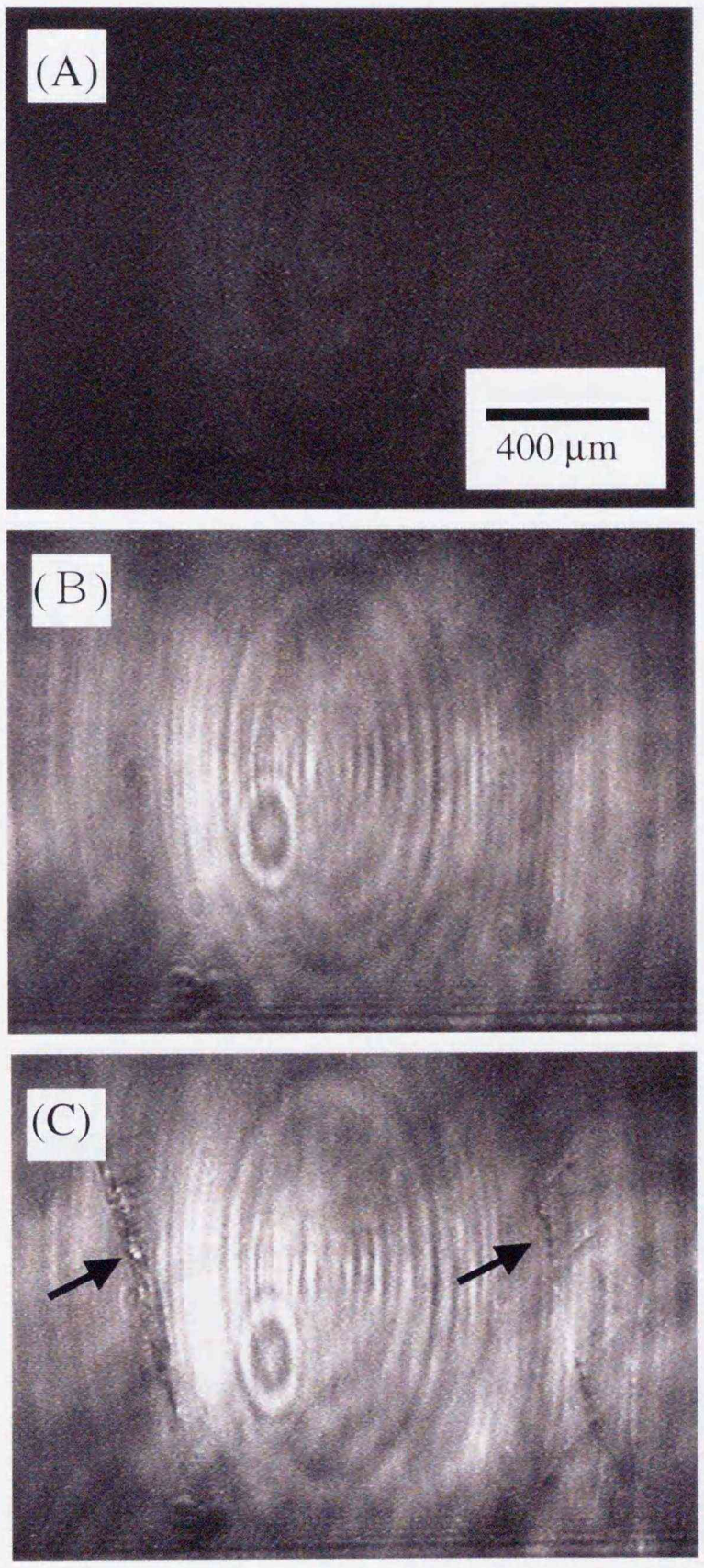

Figure 5.5 **(A)** a surface when a chloroform solution of $[Ru(phen)_2(dC18bpy)] (ClO_4)_2$ was spread onto aqueous dispersion of Sap (0.015 g/L); **(B)** the same surface compressed to 20mN m^{-1}; **(C)** the same surface compressed to 45 mN/m

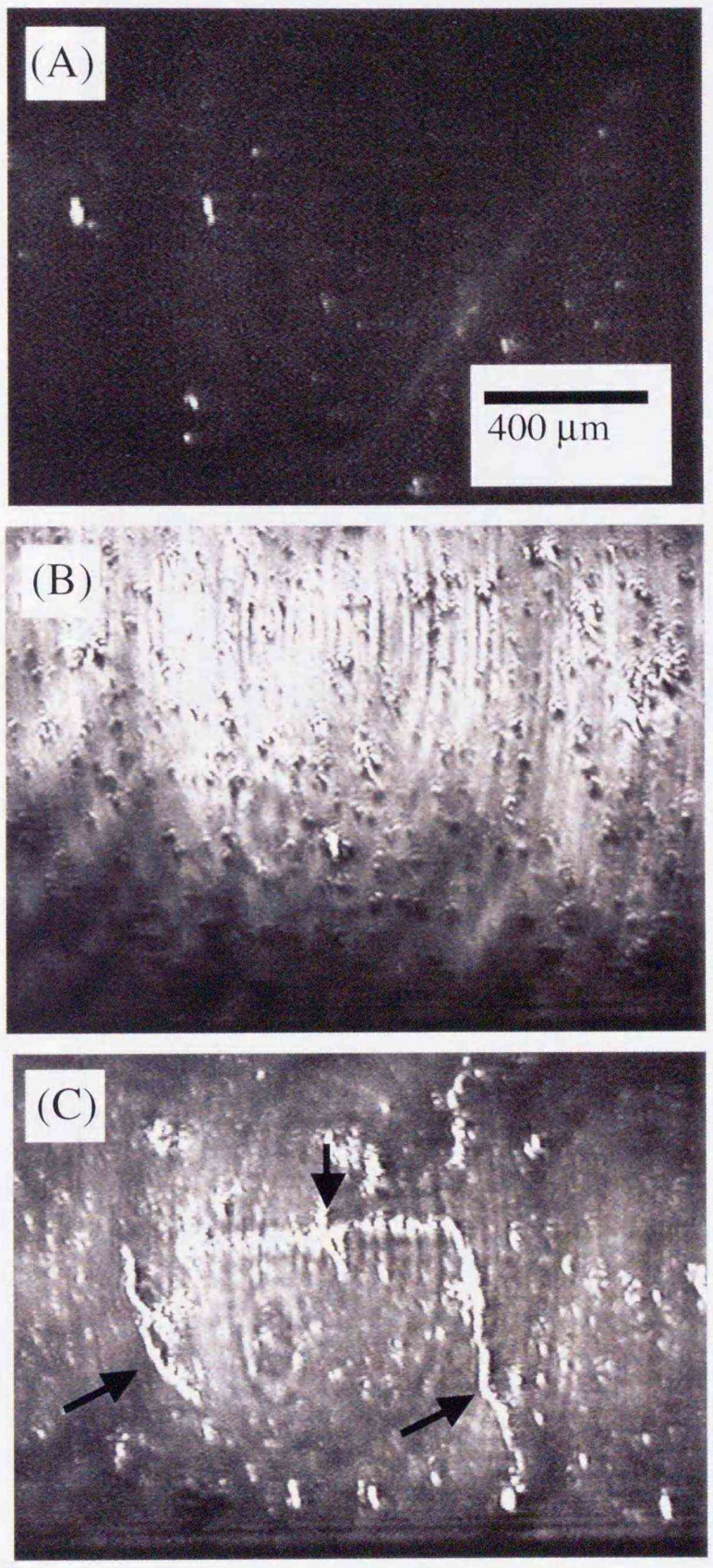

Figure 5.6 **(A)** a surface when a chloroform solution of $[Ru(phen)_2(dC18bpy)] (ClO_4)_2$ was spread onto aqueous dispersion of Li-HT (0.008 g/L); **(B)** the same surface compressed to 20 mN/m; **(C)** the same surface compressed to 45 mN/m.

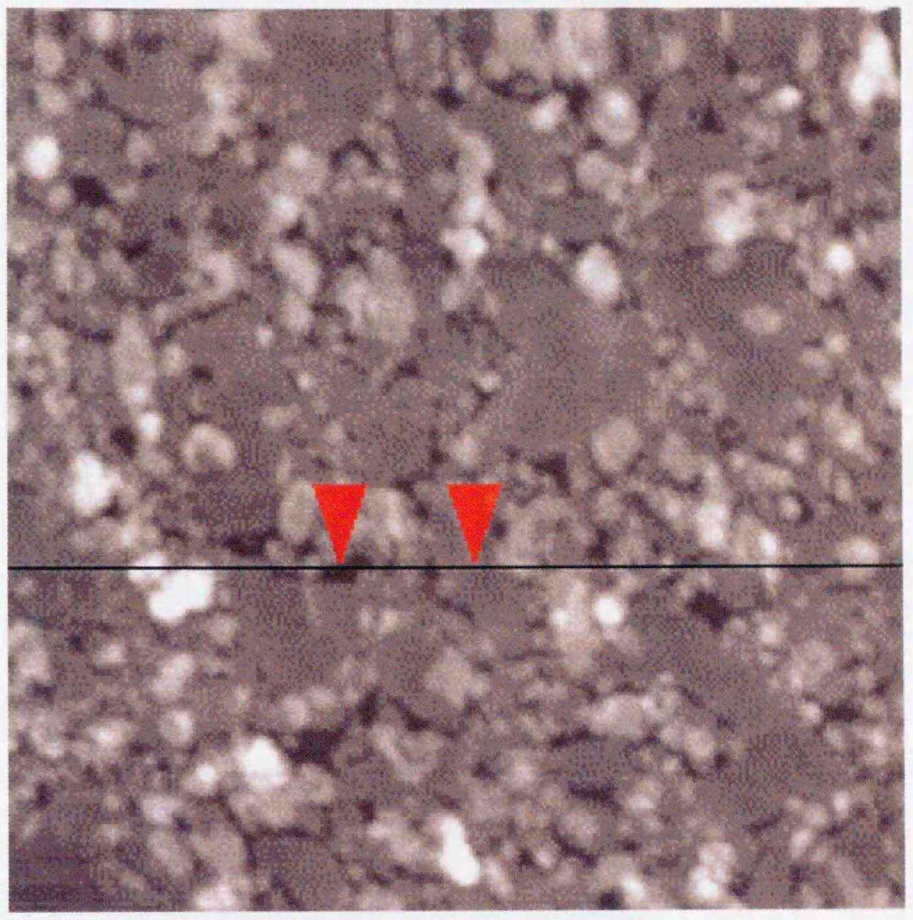

Figure 5.7 The 1.5 μm x 1.5 μm AFM image of film deposited onto a hydrophilic glass plate under the conditions of Figure 5.5 B.

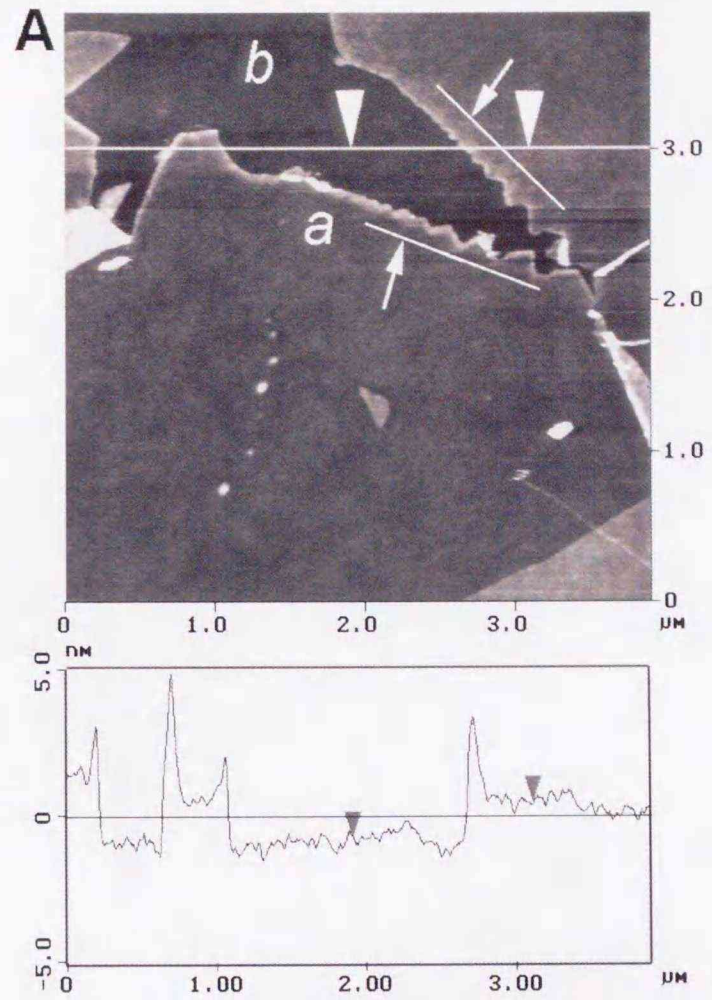

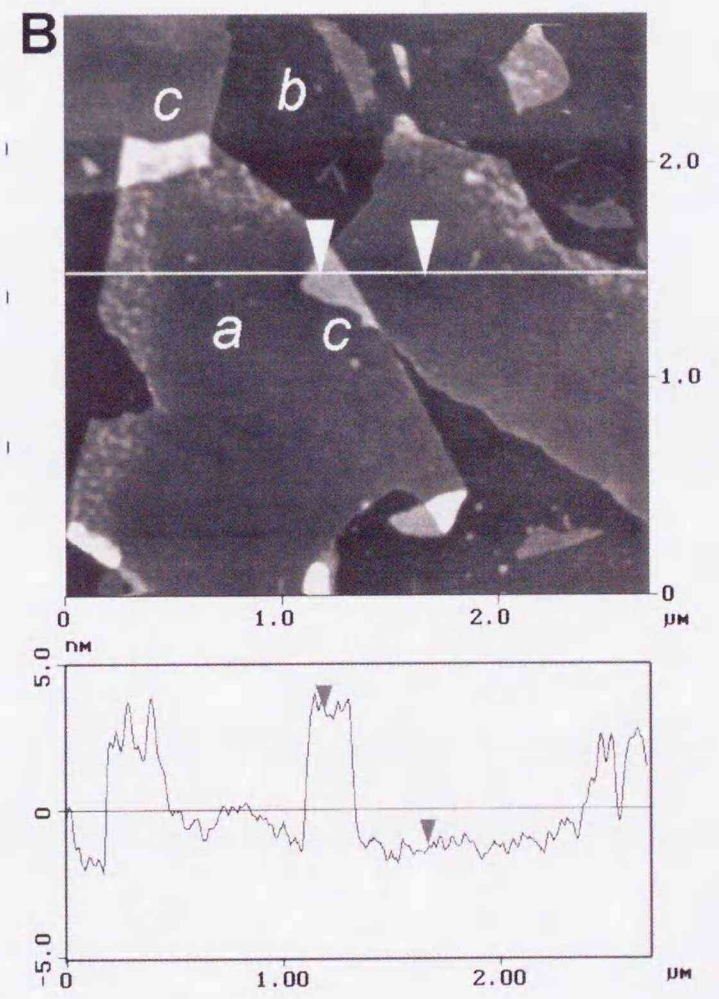

Figure 5.8 (**A**) The 4.0 μm x 4.0 μm AFM image of a film deposited onto a hydrophilic glass plate under the conditions of Figure 5.6 B; (**B**) The 2.5 μm x 2.5 μm AFM image of the same sample, showing the overlap of two layers.

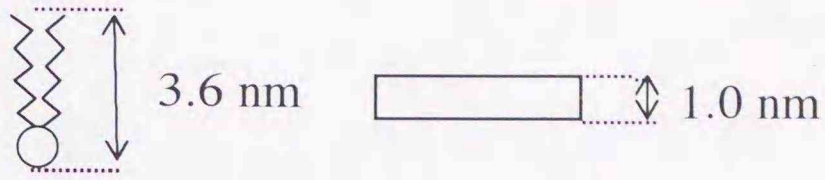

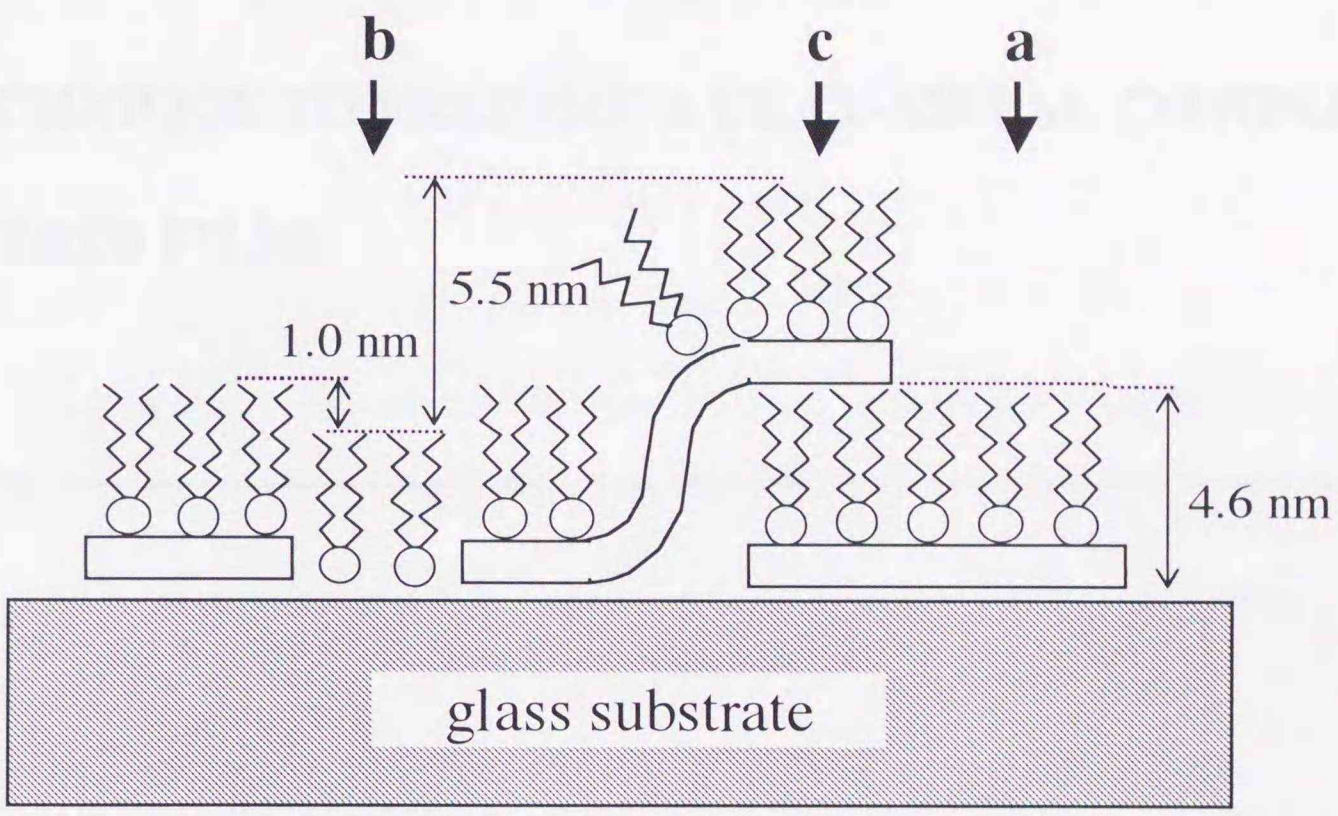

Figure 5.9 The schematic illustration of a ruthenium (II) complex-clay hybrid film (corresponding to Figure 5.8A and B).

CHAPTER 6

APPLICATION OF THE LANGMUIR-BLODGETT TECHNIQUE TO PREPARE A CLAY-METAL COMPLEX HYBRID FILM

ABSTRACT

A clay-metal complex multilayer film was prepared with the Langmuir-Blodgett technique. A monolayer of an amphiphilic ruthenium (II) complex, $[Ru(phen)_2dC18bpy)](ClO_4)_2$, (phen=phenanthroline, dC18bpy = 4,4'-dioctadecyl-2,2'-bipyridyl), was formed on an aqueous suspension of hectorite clay (Li-HT). The clay and a metal complex was transferred onto a hydrophilic glass plate to form a multilayer film of Z-type. The formation of an ordered film of $[Ru(phen)2(dC18bpy)]^{2+}$/hectorite with the layer thickness of 5.4 nm has been confirmed by X-ray diffraction, UV-visible and FT-IR absorption spectra, Brewster angle and atomic force microscopic measurements.

6.1 Introduction

Construction of organic/inorganic nanostructured materials is an important target of modern materials research. The research has been motivated by a purpose of developing functional materials such as sensors, electrode-modifiers, nonlinear optical devices and pyroelectric materials.[1-6] Of particular interest is the preparation of highly ordered organic/inorganic ultra-thin films in which an organic small molecule or a macromolecule is sandwiched between inorganic sheets. An inorganic layer is incorporated to reinforce the lamella structure of a film.

One method of preparing such a hybrid film is bond chemically an inorganic sheet to an organic anchor which is self-assembled on a solid surface.[7] Multilayer formation is accomplished by bridging neighboring layers with a bifunctional agent. Another method is to deposit a polyelectrolyte and an inorganic layer alternatively onto solid substrate by immersing the substrate into their solutions.[8] A Layer-by-layer structure is maintained by electrostatic intercalation between oppositely charged layers.

Although the classical Langmuir-Blodgett (LB) technique is a powerful approach to construct multilayer molecular assemblies,[9] the method unfortunately suffers from critical drawbacks such as mechanical weakness and sensitivity to contaminates. Recently we have applied the LB method to prepare the thin films of inorganic materials and metal complexes.[10] As an extension of the work, we have shown that an ultra-thin hybrid film of a clay mineral and an amphiphilic metal complex can be built by

using the LB technique. According to the method, a monolayer of an amphiphilic Ru(II) complex was formed onto an aqueous dispersion of a clay. The monolayer was used as template for adsorption of a clay particle.

A ruthenium(II) complex, $[Ru(phen)_2dC18bpy)](ClO_4)_2$, (phen=1,10-phenanthroline, dC18bpy = 4,4'-dioctadecyl-2,2'-bipyridyl) (shown by Figure 5.1), was used as an amphiphilic compound. The optical isotherms of the compounds were obtained in a highly purified form. Ruthenium(II) polypyridyl complexes are known to be an efficient converter of photon energy.[11] Such a new hybrid film could be an important step towards the creation of organized layered compounds for controlling the deposition sequence and orientation of intercalated molecules.

6.2 Experimental

***Materials*:**

$[Ru(phen)_2dC18bpy]^{2+}$ was prepared by refluxing $[Ru(phen)_2Cl_2]$ (50mg) and dC18bpy (70mg) with $AgNO_3$ (32mg) in 20 ml of an ethanol solution for 20 min. An orange precipitate was formed by adding $NaClO_4$ to the reactant mixture. A perchlorate anion was replace by mixing $[Ru(phen)_2dC18bpy](ClO_4)_2$ with an anion exchange resin of Cl^- type. Resolution of $[Ru(phen)_2dC18bpy]^{2+}$ was performed by adding 0.1 g of sodium antimonyl tartrate salt to 20 mL of a 1 : 1 water - ethanol (v/v) solution of the racemic $[Ru(phen)_2dC18bpy]Cl_2$. Δ-$[Ru(phen)_2dC18bpy]^{2+}$ was filtered off as an insoluble antimonyl tartrate salt. The anion of the salt was converted

to the perchlorate by use of an anion-exchange resin. Λ-[Ru(phen)$_2$dC18bpy] (ClO_4)$_2$ was obtained by adding an excess amount of sodium perchlorate to the filtrate. The CD spectra of Δ– and Λ– enantiomers gave De =324 and -330 at 281 nm, respectively. The optical purity of both enantiomers was estimated to be higher than 95 %.

Clay used is a synthetic lithium hectorite (Li-HT, Topy Industries Co.,Ltd) with the composition of $Li^+_{0.60}(Mg_{1.40}Li_{0.60})Si_4O_{10}F_2$. The cation exchangeable capacity (CEC) was determined to be 140 meq/100g by Ca^{2+} adsorption method. It was dispersed by stirring for 1 day in distilled water and adjusted to 80 mg/l.

Instruments

Surface pressure - area (π-A) curves were measured with a Langmuir trough (U.S.I.Co. Ltd., Japan). A π-A curves was recorded 30 minutes after a chloroform solution of a metal complex was spread onto water surface. The rate of compression was 10 cm^2/min. A LB film was prepared by a vertical dipping method at the dipping rate of 10 mm/min. Brewster angle microscopy (BAM) experiments were performed with an instrument constructed by Dr. H.Yokoyama (Electotechinical Laboratory, Japan). Reflected laser light passed though a lens onto CCD camera and the resulting video signal was fed to a video system. Atomic force microscopic (AFM) images were recorded at room temperature in air with a Nanoscope III scanning probe microscope (DI Instruments, USA). Nanoprobe integral cantilevers (Si_3N_4) were used, having tips with a spring contact of 0.06 nm^{-1} (Park Scientific). The AFM images were obtained in the tapping mode with filters off. The 'd' scan head was used, which has a

maximum scan range of 12 μm by 12 μm by 4.4 μm.

6.3 Results and Discussion

Monolayer Behaviors

Curves (a) - (c) in Figure 6.1 show the surface pressure versus molecular area (π-A) isotherms when 100 - 300 μl of 6.1×10^{-5} M chloroform solutions of racemic $[Ru(phen)_2(dC18bpy)](ClO_4)_2$ were spread on an aqueous 0.1 M $NaClO^4$ solution. Surface pressure rose from zero at 1.2 nm^2/molecule and increased steeply until it attained a plateau above 50 mN/m. The lift-off area was nearly equal to the cross sectional area of the head group of the complex (1.5 nm^2/molecule). The result indicated that the molecule formed a closely packed monolayer and collapsed at the surface pressure above 50 mN/m. Comparing the isotherms between racemic and enantiomeric $[Ru(phen)_2(dC18bpy)]^{2+}$, it was concluded that packing density was a little higher in the heterochiral monolayer than in the homochiral one.[10b]

Curves (d) - (f) in Figure 6.1 are isotherms when 75 - 125 μl of 8.4×10^{-5} M chloroform solutions of $[Ru(phen)_2(dC18bpy)](ClO_4)_2$ were spread on an aqueous suspension of Li-HT (0.008g/l). These curves displaced by 1 nm^2 towards the larger molecule area than curves (a) - (c), supporting the interaction of a clay layer with a cationic monolayer. The isotherm attained a plateau at the molecular area of 1.2 nm^2. On the basis of the elemental compositions of Li-HT (given in the experimental section), an area of 1.2 nm^2 is estimated to carry a negative charge of -2.2 e, which was nearly

compensated by the charge of the divalent metal complex. The results indicated that adsorption took place according to ion-exchange mechanism.

Interaction of a clay with a floating molecular was studies *in situ* with a Brewster angle microscope (BAM). When racemic $[Ru(phen)_2(dC18bpy)](ClO_4)$ was spread on an aqueous 0.1 M $NaClO_4$ solution, a bright region with a size of a few thousand micrometers was observed to float water surface. It implied that the complex formed a monolayer island even at zero surface pressure. The whole surface was uniformly bright at 30 mN/m, indicating that the surface was completely covered with a monolayer (Figure 5.4B). When surface pressure exceeded 50 mN/m, there appeared an intensity bright straight line that expended over a few thousand micrometers (Figure 5.4C). It indicated the collapse of the monolayer to result in a multilayer or a micro-crystalline. When the same metal complex was spread on an aqueous suspension of Li-HT (0.008 g/l), bright spots with a radii of 10 - 100 μm were seen at zero surface pressure (Figure 5.6A). These spots were undoubtedly due to clay particles adsorbed to the monolayer islands a metal complex. The density of spots increased on compressing a surface until the whole surface was covered with spots at 30 mN/m (Figure 5.6B). When surface pressure exceeded 40 mN/m, bright lines appeared in a zigzag way, indicating the collapse of a film (Figure 5.6C).

Multilayer Properties

Monolayers could be efficiently deposited onto a solid substrate such as a hydrophilic glass plate and a silicon wafer. Deposition took place only in the upwards direction (Z-type deposition). A film is denoted as [Ru]/[$NaClO_4$] or [Ru]/[Li-HT]

when a monolayer of racemic $[Ru(phen)_2(dC18bpy)]^{2+}$ was deposited from an aqueous $NaClO_4$ solution or an aqueous Li-HT deposition, respectively. Dotted and solid curves in Figure 6.2 show XRD patterns for [Ru]/[$NaClO_4$] (10 layers) and [Ru]/[Li-HT](7 layers) transferred onto a hydrophilic quartz at 20 mN/m, respectively. Basal spacing was determined to be 4.2 and 5.3 nm for [Ru]/[$NaClO_4$] and [Ru]/[Li-HT], respectively. For the former, the basal spacing was nearly equal to the sum of the molecular height of $[Ru(phen)_2(dC18bpy)]^{2+}$ (3.6 nm) and diameter of ClO_4^- (0.5 nm)[12] or 4.1nm. For the latter, basal spacing was 0.7 nm larger than the sum of the molecular height of $[Ru(phen)_2(dC18bpy)]^{2+}$ (3.6 nm) and the thickness of a single clay layer (1.0 nm)[13] or 4.6 nm. Thus the film was probable to include either a double clay layer or other kinds of counter cations absorbed on the opposite side of a clay layer.

Polarized electronic absorption spectra were measured for [Ru]/[Li-HT](5 layers) deposited on a hydrophilic quartz substrate. Figures 6.3a and b show the spectra when transversely and perpendicularly polarized lights were incident on the sample at an angle of 45°, respectively. It was seen that the absorption band at 460 - 430 nm, which was assigned to the metal-to-ligand charge transfer (MLCT) band,[14] showed dichroic effect. A dichoic ratio, $A_{\parallel}/A_{\perp}$, was given by the following equation:[10d]

$$A_{\parallel}/A_{\wedge} = \frac{\frac{1}{2}\sin^2\alpha}{\frac{1}{2}\sin^2\alpha\cos^2\phi + \cos^2\alpha\sin^2\phi}$$

in which α and ϕ denote the angle of transition moment and incident light with respect to the normal direction of a substrate. In the present measurement, ϕ was taken to be

45°. Assuming that the band mainly arose from the MLCT transitions to two 1,10-phennanthroline ligands, the dichoic ratio was calculated to be 1.25 when a metal complex oriented its alkyl chains normal to a surface (or a α was 120°). The prediction agreed well with the observed dichroic ratio of 1.30 -1.50 over the band.

Dotted and solid curves in Figure 6.4 show infrared adsorption spectra for [Ru]/[$NaClO_4$](10 layers) and [Ru]/[Li-HT](7 layers) transferred onto a silicon wafer, respectively. Peaks at 2923 cm^{-1} and 2852 cm^{-1} or the asymmetric and symmetric stretching vibrations of methylene groups of dC18bpy ligands, respectively, were seen in both samples, while peaks at 1004 cm^{-1} and 467 cm^{-1}, which were assigned to the Si-O-Si stretching bands in Li-HT, were seen only for [Ru]/[Li-HT].[15] These experiments proved the existence of a clay layer within the LB films and the well-defined lamella structure of the built-up films.

Surface Structures

The deposition state of a clay sheet was investigated with an atomic force microscope (AFM). Figure 5.8A (in Chapter 5) shows the AFM image of a floating film deposited onto a hydrophilic glass plate in the upwards direction under the conditions of Figure 5.6B. A surface was covered with planar particles (dotted by **a**). There was a lower part (dotted by **b**) among the particles. The surface of **a** was estimated to be 1.5 × 0.5 nm higher than that of **b**. The value was comparable to the difference of basal spacing (1.1 nm) between [Ru]/[$NaClO_4$](4.2 nm) and [Ru]/[Li-HT](5.3 nm) as determined by X-ray measurements. In the image of a different part (Figure 5.8B), particles were partially overlapped to form a double layer as indicated by

c. The thickness of the upper layer was estimated to be 5.0 ± 1.0 nm. The value was comparable to the basal spacing of [Ru]/[Li-HT] (5.3 nm).

The above AFM results were consistent with a view that parts **a**, **b** and **c** were a monolayer of $[Ru(phen)_2(dC18bpy)]^{2+}$/hectorite, a monolayer of $[Ru(phen)_2(dC18bpy)](ClO_4)_2$ and a double layer of $[Ru(phen)_2(dC18bpy)]^{2+}$/hectorite, respectively. Notably the double layer regions (**c**) were connected smoothly with single layer regions **(a)**, implying that the clay layer was so flexible to change its shape according to the up-and-down of an underneath surface.[16] More interestingly there were two facing particles whose rough edges seemed to compensate each other (indicated by two arrows in Figure 5.8A). It implied that these were originally parts of the same layer but they were torn into two fragments during deposition. Figure 5.8C shows the image of a larger crystal. There were aggregated regions observed near an edge. It indicated that same metal complexes were not fixed on a clay surface but moved to form an aggregate. It is not clear what kind of property was responsible for the mobility of a metal complex on a clay surface. For comparison, an aqueous suspension of Li-HT (0.008 g/l) was cast on a glass plate and dried. The AFM of the surface indicated that most of clay particles were aggregated to form large domains with a few hundred nanometers in size and tens of nanometers in height. In rare cases, an isolated clay particle was observed as shown in Figure 5.8B . The thickness of a particle was estimated to be 1.5 ± 0.5 nm, indicating that it was either a single or double layer.

6.4 Conclusion

We have used the adsorption of a clay layer on a positively charged monolayer of $[Ru(phen)_2(dC18bpy)]^{2+}$ and the Langmuir-Blodgett technique to construct new organic/inorganic nano-structured films. Currently we are investigating the effect of the size and charge density of a clay layer for various kinds of natural and synthetic clay minerals. The preliminary results indicate that the method described in this work can be extended to all types of clay minerals to give rise to new lamella organized materials. Appropriate choice of clay minerals and amphiphilic compounds allows LB films having particular optical and electrochemical properties to be constructed.

References

[1] Lvov, Y.; Ariga, K.; Ichinose, I.; Kunitake, T. *Langmuir.* **1996,** *12,* 3038.

[2] Kotov, N.A.; Haraszi, T.; Turi, L.; Zavala, G.; Geer, R.E.; Dèkàny, I.; Fendler, J.H. *J. Am. Chem. Soc.,* **1997,** *119,* 6821.

[3] Ichinose, I.; Kimizuka, N.; Kunitake, T. *J. Phys.Chem.* **1995,** *99,* 3736.

[4] Tsutsumi, N.; Sakata, K.; Kunitake, T. *Chem.Lett.* **1992,**1465.

[5] Swalen, J.D.; Allara, D.L.; Andrade, J.D.; Chandross, E.A.; Garoff, S.; Israelachvili, J.; McCarthy, T.J.; Murray, R.; Pease, R.F.; Rabolt, J.F.; Wynne, K.J. *Langmuir.* **1987,** *3,* 932.

[6] Kotov, N.A.; Dèkàny, I.; Fendler, J.H. *J. Phys. Chem.,* **1995,** *99,* 13065.

[7] Rong, D.; Kim, Y.; Mallouk, T.E. *Inorg. Chem.* **1990,** *29,* 1531.

[8] Kleinfeld, E.R.; Ferguson, G.S. *Science.,* **1994,** *265,* 370.

[9] *Insoluble monolayers at Liquid-Gas Interfaces* ; Gaines, G.L..Jr.; Interscience Publishes: New York, 1996.

[10] (a) Inukai, K.; Hotta, Y.; Taniguchi, M.; Tomura,A.; Yamagishi, A. *J. Chem. Soc., Chem. Commun.,* **1994,** 959. (b) Yamagishi, A.; Goto, Y.; Taniguchi, M. *J. Phys. Chem.,* **1994,** 100, 1827. (c) Yamagishi, A.; Sasa, N.; Taniguchi, M. *Langmuir,* **1997,** 13, 1689. (d) Aramata, K.; Kamachi, M.; Takahashi, M.; Yamagishi, A. *Langmuir,* **1997,** 13, 5161. (e) Hotta, Y.; Inukai, K.; Taniguchi, M.; Yamagishi, A. *J. Electroanal. Chem.* **1997,** 429, 107. (f) Kashiwara, S.; Takahashi, M.; Nakamura, M.; Taniguchi, M.; Yamagishi, A. *Journal of Material Chemistry,* **1998** (in press).

[11] Rotzinger, F.P.; Munavalli, S.; Comte, P.; Hurst, J.K.; Gratzel, M.; Pern, F.; Franck, A.J. *J. Am. Chem. Soc.,* **1987,** 109, 6619.

[12] *Chemistry of the Elements* ; Greenwood, N.N.; Earnshaw, A.; Butterworth-Heinemann: Oxford, 1984.

[13] *Crystal Structures of Clay Minerals and their X-ray Identification* ; Brindley, G.W.; Brown, G.; Mineralogical Society: London, 1980.

[14] Riesen, H.; Wallace, L.; Krausz, F. *J. Phys. Chem.* **1996,** *100,* 17138.

[15] Sutubican, V.; Roy, R. *J. Am. Ceram. Soc.* **1961,** *44,* 625.

[16] Nakazawa, H.; Yamada, H.; Fujita, T. *Appl. Clay. Sci.* **1992,** *6,* 395.

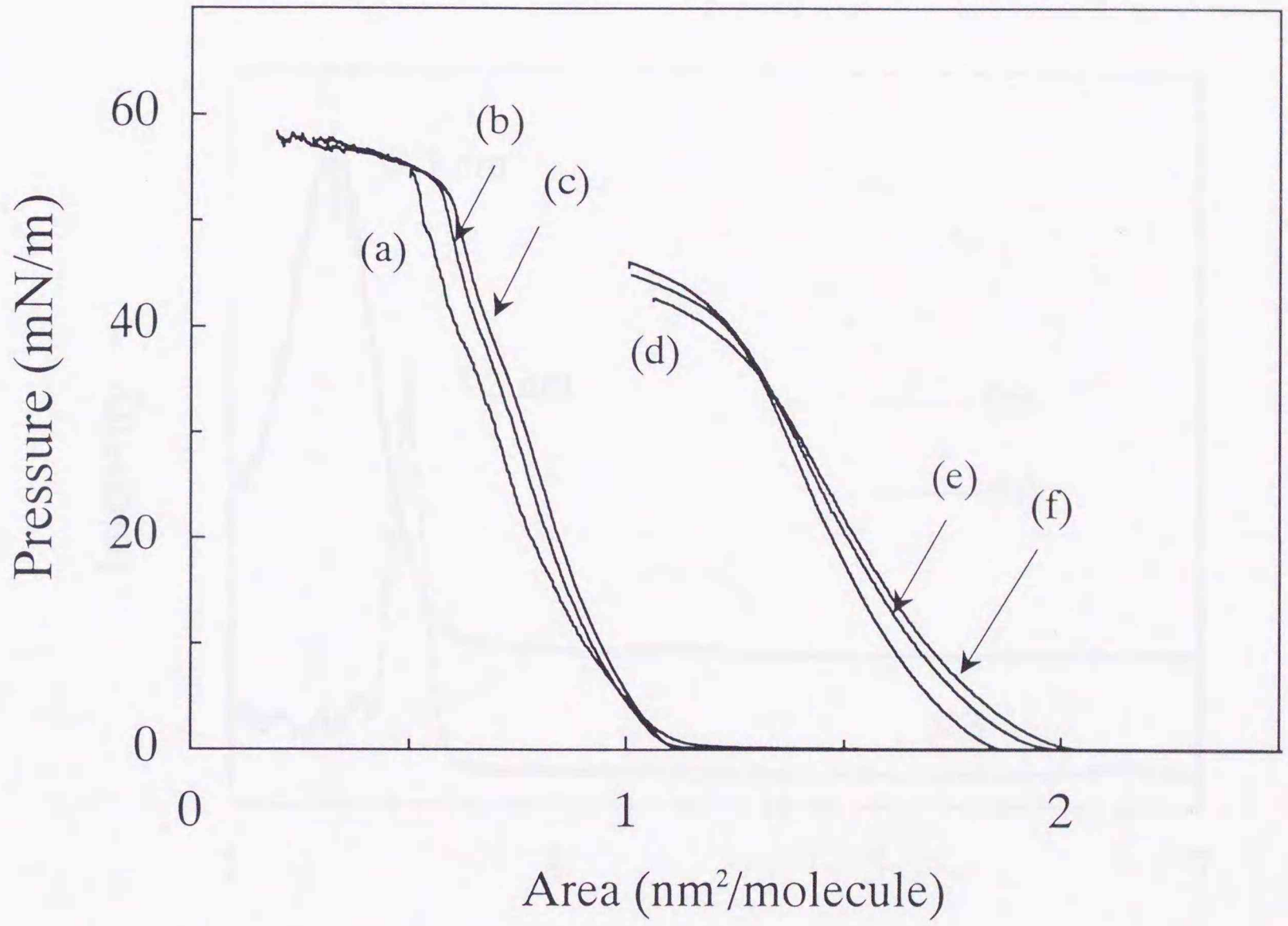

Figure 6.1 Surface pressure-molecular area (π-A) curves at 25°C when **(a)**100, **(b)**200 and **(c)**300 μL of a 2×10^{-4} M a chloroform solution of $[Ru(phen)_2(dC18bpy)](ClO_4)_2$ were spread onto an aqueous 0.1 M $NaClO_4$ solution or **(d)** 75, **(e)** 100 and **(f)** 125 μL of a 8.4×10^{-4} M a chloroform solution of the same complex were spread onto an aqueous suspension of Li-HT (0.008 g/l).

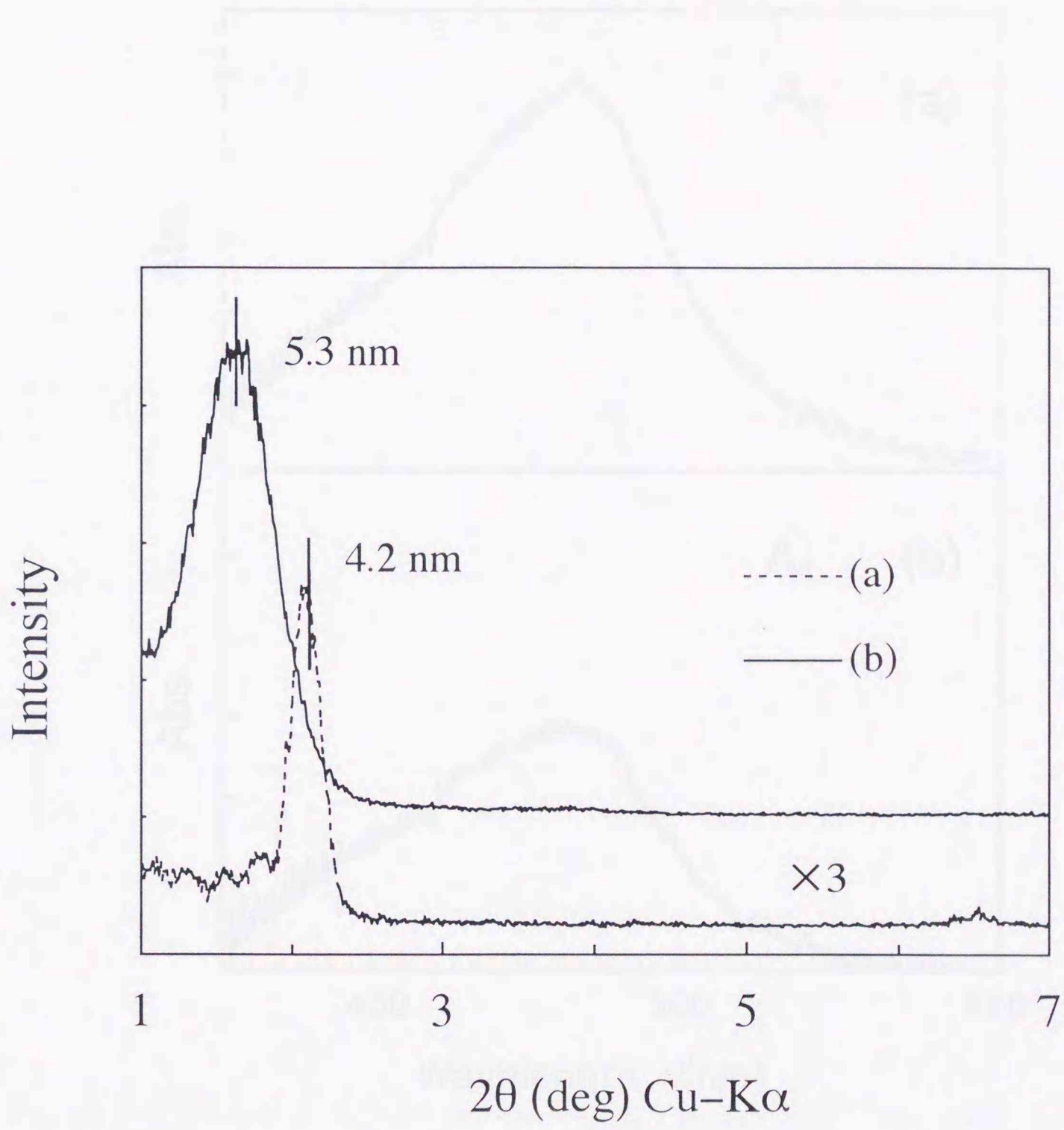

Figure 6.2 XRD patterns for **(a)** [Ru]/[Li-HT] (7 layers) and **(b)** [Ru]/[$NaClO_4$] (10 layers) transferred onto a hydrophilic quartz at 20 mN/m, respectively.

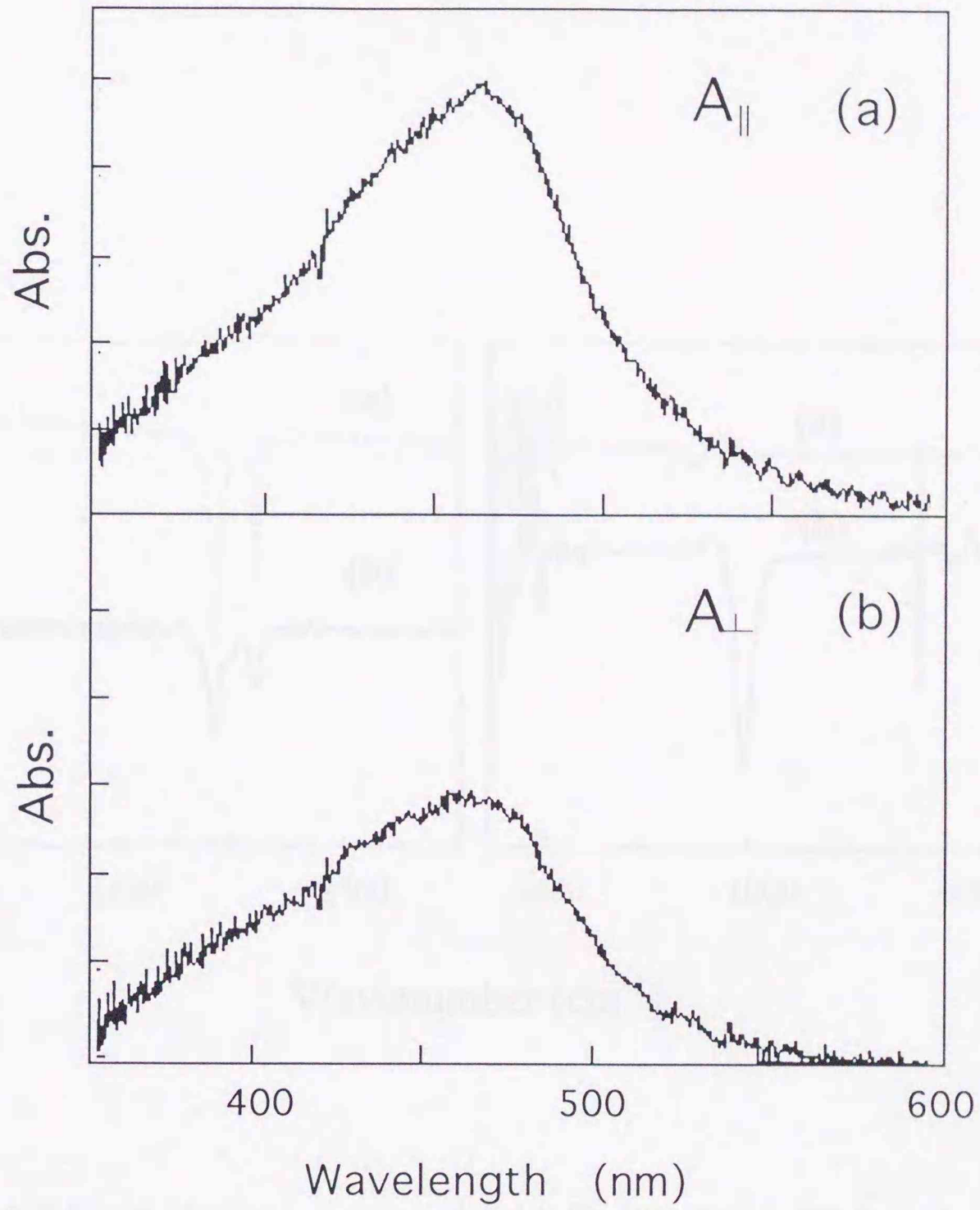

Figure 6.3 Polarized electronic absorption spectra for [Ru]/[Li-HT] (5 layers) deposited on a hydrophilic quartz substrate, when **(a)** transversely and **(b)** perpendicularly polarized lights were incident on the sample at an angle of 45°, respectively.

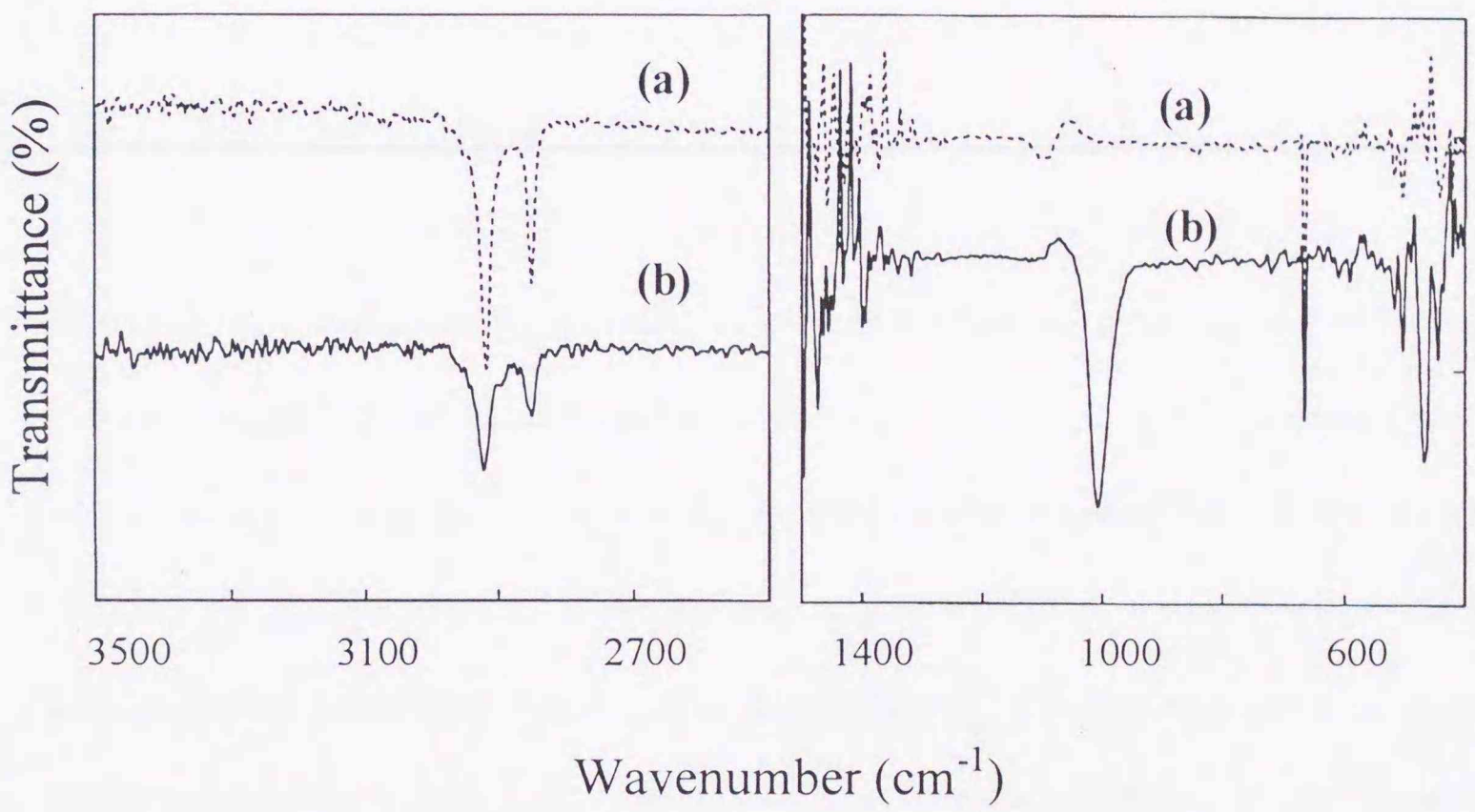

Figure 6.4 Infrared absorption spectra for **(a)** [Ru]/[$NaClO_4$] (10 layers) and **(b)** [Ru]/[Li-HT] (7 layers) transferred onto a silicon wafer.

CHAPTER 7

GENERAL CONCLUSIONS

In this thesis, we have first studied the swelling properties of bulk clay minerals. Next, on the basis of the above results, we have developed the formation of layer-by-layer structures of clay-organic hybrid films at an air-water interfaces using the classical Langmuir-Blodgett (LB) technique.

In Chapter 2, the hydration behavior of high crystallinity smectite (HCSm) with various exchangeable cations was observed by in situ XRD measurements under controlled relative humidity (RH). The basal spacing of HCSm varied stepwise with increasing RH, except for the **R**-phase, a random interstratified structure of **1W** (1-layer hydration state) and **2W** (2-layer hydration state). Coexistence of two hydration states was observed in the XRD patterns as an (001) reflection doublet. These results clarified the stoichiometric hydration of the ideal smectite having a homogeneous charge distribution in the silicate layer. The appearance of the **R**-phases was a kinetic phenomenon in the hydration and dehydration processes which was largely controlled by the hydration force of cations in the interlayer.

In Chapter 3, the swelling properties of the colloidal taeniolite suspensions were investigated by *in situ* XRD techniques. With increasing water, *00l* reflections shifted to a very low angular range and the local background intensity at small angles increased simultaneously. The line profile of the swelling Li-TN showed higher order reflections throughout the swelling progress. The degree of the parallel alignment of clay sheets becomes more regular with increasing water contents, and up to fifth ordered reflections were observed. The profile analyses using Laue function indicated that the wavy

reflections observed implied a pair of taeniolite sheets incorporating water and that the nanosheets was so flexible to change its shape by the diffusion of water molecules.

In Chapter 4, lithium taeniolite (Li-TN) and lithium hectorite (Li-HT) form intercalation complexes with TMA having different chain lengths. With increasing exchange ratio of TMA^+/ Li^+ the complexes initially take regularly and randomly interstratified structures with layer units of TMA and water intercalated layers. Finally the complexes take a "paraffin - type bilayer structure", where the long chain of TMA inclines at about 30° to the silicate sheet. Li-HT and Li-TN showed quite similar intercalation characteristics, but Li-TN is the better host as demonstrated by the narrower FWHM of the (001) reflections and by the sharper transition from the regularly and randomly interstratified complexes to the final structure. The difference can predominantly be attributed to higher layer charge and crystallinity of Li-TN.

In Chapter 5, the effects of the particle size and charge density of smectite on the formation of a LB hybrid thin film have been investigated by Brewster angle microscope (BAM) and atomic force microscope (AFM). As a result, an ultrathin film was constructed by fixing an amphiphilic ruthenium complex to a rigid inorganic sheet. A clay layer may have a role to enhance the mechanical strength of a film and to fix an adsorbed molecule in two-dimensional regularity. Hybridization is facilitated by electrostatic anchoring of the cationic head group of a metal complex onto the anionic sheet of a clay. Appropriate choice of smectites and amphiphilic compounds allows LB films of uniform thickness to be constructed.

In Chapter 6, the monolayer of a clay and a metal complex is transferred onto a hydrophilic glass plate to form a multilayer film of Z-type. The formation of an

ordered film of $[Ru(phen)_2(dC18bpy)]^{2+}$/hectorite has been confirmed by X-ray diffraction, UV-visible and FT-IR absorption spectra. The results indicate that the method described in this work can be extended to all types of clay minerals to give rise to new lamella organized materials. Appropriate choice of clay minerals and amphiphilic compounds allows LB films having particular optical and electrochemical properties to be constructed.

These results suggest an essential ingredient for controlling and designing a construction of layer-by-layer nanostructured material. The role of an inorganic layer is to enhance the mechanical strength of a film and to fix an attached molecule in two-dimensional regularity. A ruthenium(II) polypyridyl complex was used as an amphiphilic compound since the molecules are efficient in converting photo-energy to chemical energy. The obtained hybrid film would be of promising value as a light-harvesting system or a non-linear optical materials or an electrode modifier. These possibilities will evoke an interest in relevant fields such as photochemistry, electrochemistry and surface science.

List of Publication

(1) **Intercalation of N-Alkyltrimethylammonium into Swelling Fluoromica** K. Tamura and H. Nakazawa, *Clays and Clay Minerals,* **44,** 501-504 (1996).

(2) **A Clay-Metal Complex Ultrathin Film as Prepared by the Langmuir-Blodgett Technique** K. Tamura, H. Setsuda, M. Taniguchi and A. Yamagishi, *Chemistry Letters*, 121-122 (1999).

(3) **Formation of Layer-by-Layer Composite Films by the Langmuir-Blodgett Technique: Smectite-Amphiphilic Ruthenium (II) Complex systems** K. Tamura, H. Setsuda, M. Taniguchi, M. Takahashi and A. Yamagishi, *Clay Science*. (1999 in press)

(4) **Application of the Langmuir-Blodgett Technique to Prepare a Clay-Metal Complex Hybrid Film** K. Tamura, H. Setsuda, M. Taniguchi, M. Takahashi and A. Yamagishi, *Langmuir.* (to be submitted)

(5) **Hydration Behavior of High Crystallinity Smectite with Different Exchangeable Cations** K. Tamura, H. Yamada and H. Nakazawa, *Clays and Clay Minerals.* (to be submitted)

(6) **Laue Function Analysis of Colloidal Lithium Taeniolite** K. Tamura, T. Sasaki, H. Yamada and H. Nakazawa, *Langmuir.* (to be submitted)

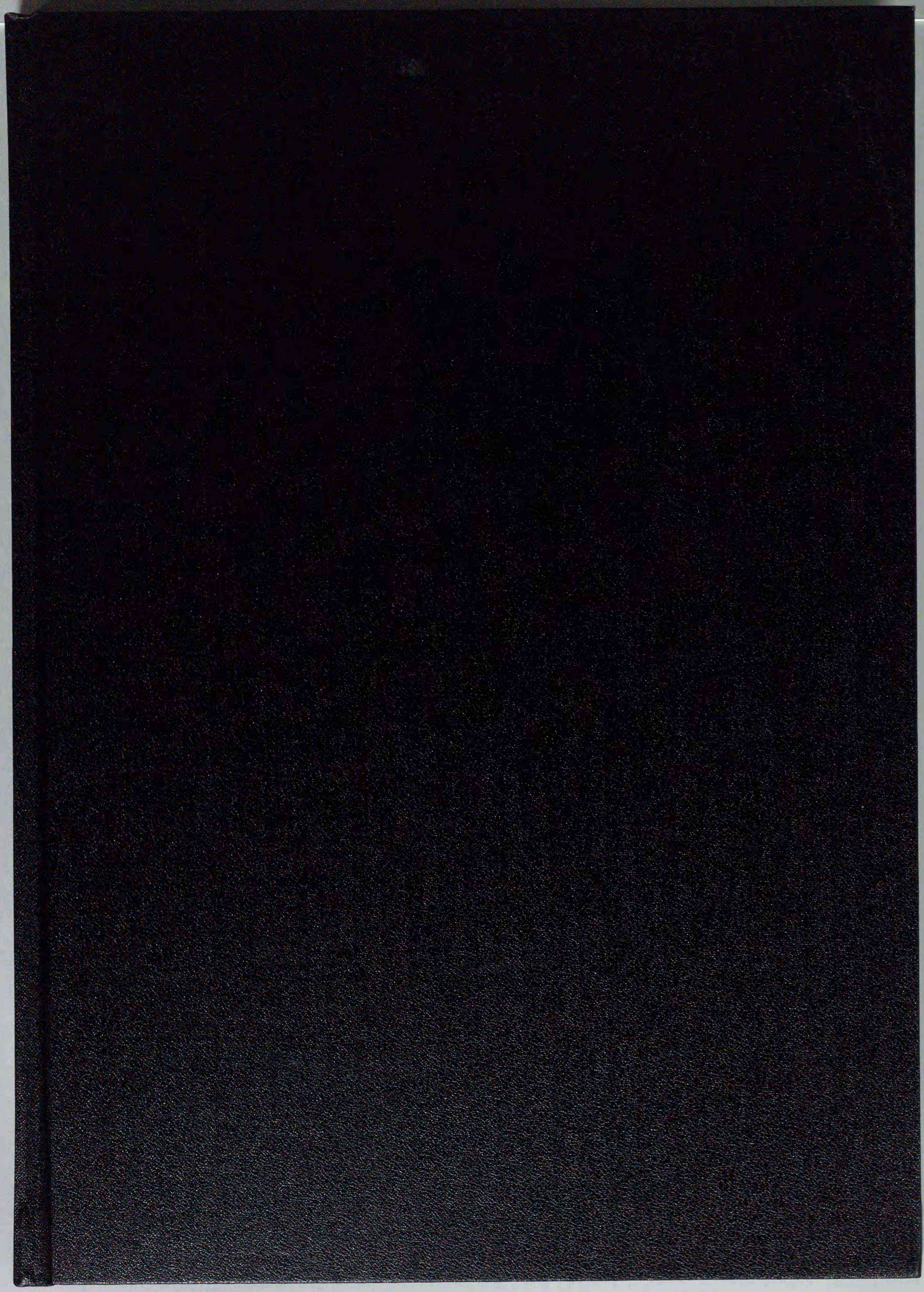

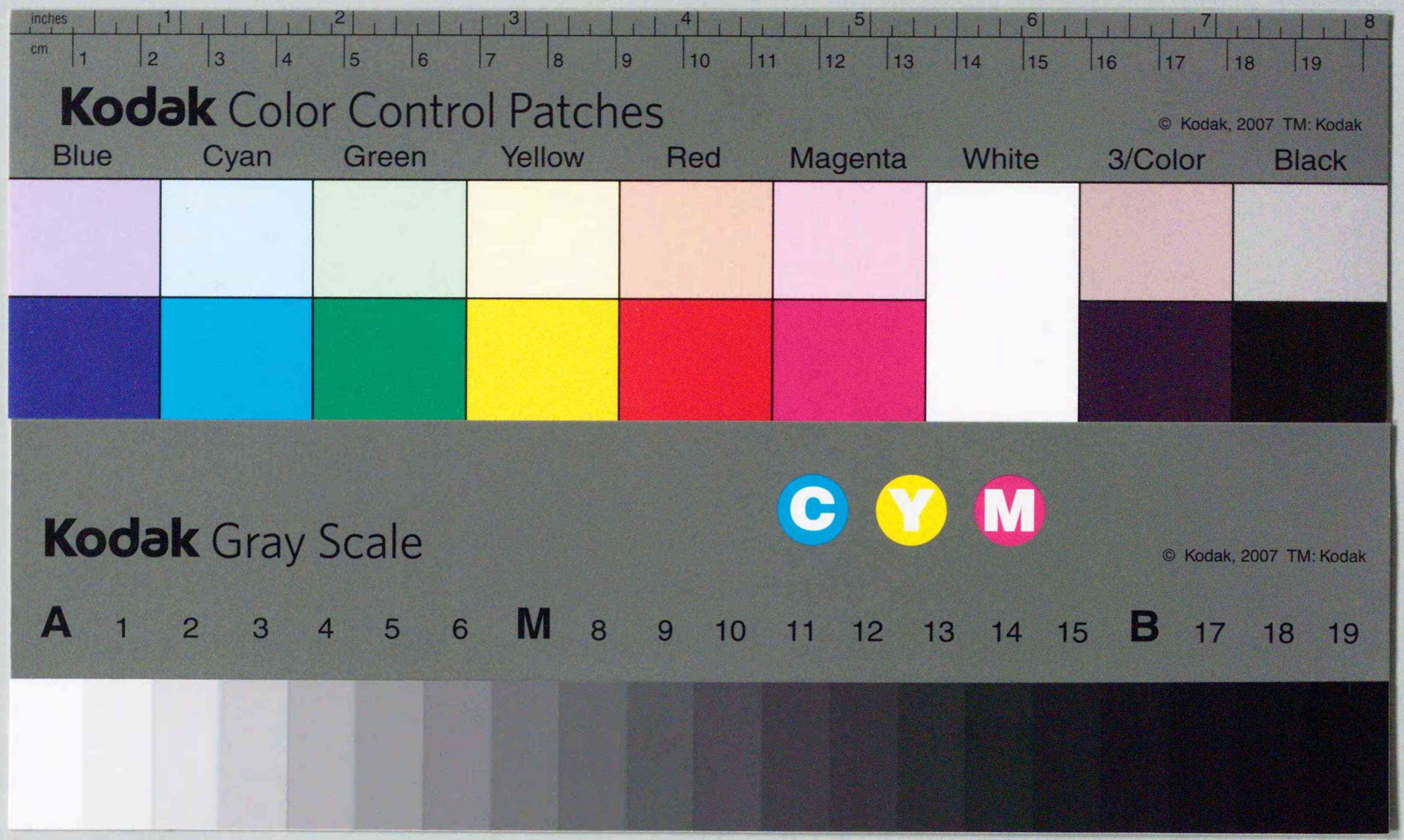
inches
cm
Kodak Color Control Patches
© Kodak, 2007 TM: Kodak
Blue
Cyan
Green
Yellow
Red
Magenta
White
3/Color
Black
Kodak Gray Scale
C
Y
M
© Kodak, 2007 TM: Kodak
A 1 2 3 4 5 6 M 8 9 10 11 12 13 14 15 B 17 18 19